Average-chain behavior of isotropic incompressible polymers obtained from macroscopic experimental data. A simple structure-based WYPiWYG model in Julia language

Víctor Jesús Amores, José María Benítez, Francisco Javier Montáns[*]

Escuela Técnica Superior de Ingeniería Aeronáutica y del Espacio
Universidad Politécnica de Madrid
Plaza Cardenal Cisneros, 3, 28040-Madrid, Spain

Abstract

Elastomeric materials and soft biological tissues are made up of synthetic and protein fibers, respectively. The uncoiling of these fibers during loading produces a non-linear elastic macroscopic behavior in the regime of finite strains. Many hyperelastic models have been developed to reproduce this behavior assuming the existence of a strain energy function. In structure-based models, the analytical energy function is obtained from the stored energy of all the material constituents. This stored energy is given frequently by the entropy of the chain network obtained from Langevin statistical treatment of the possible configurations adopted by the chains, and a representative cell for their spatial distribution. One of the most used models is the eight chain model, being its salient feature that it reproduces the overall response of isotropic hyperelastic materials with only two material parameters obtained from a tensile test. On the other hand, in WYPiWYG hyperelasticity the stored energies are numerical instead of analytical and capture, to any precision, the experimental tests on the material. However, due to their phenomenological nature, their determination requires more tests. In this work, we develop a microstructure-based WYPiWYG hyperelastic model in which the average chain behavior is obtained from macroscopic tests through a simple automatic inverse procedure. We show that, without assuming a probability distribution function nor any particular chain arrangement, we obtain, at the same computational cost, better predictions than the 8-chain model. Code of the model and of the examples in the Julia programming language are included.

---

[*]Corresponding author
Email address: `fco.montans@upm.es` (Francisco Javier Montáns)

1. Introduction

During small elastic deformations, stresses and strains in a material are usually related through a linear relation [1]. However, because configurational entropy governs their behavior, polymer-like materials as elastomers or soft biological tissues exhibit a highly non-linear elastic behavior, sustaining very large strains [1, 2, 3, 4, 5]. Truly elastic behavior is characterized by the absence of dissipation during any type of loading, e.g. cyclic loading [6, 7]. The hypoelastic nonlinear relations (extending the small strain linear framework to nonlinear relations), do not guarantee conservative behavior [8, 7] unless some integrability conditions due to Bernstein are fulfilled [9, 10]. These conditions guarantee the existence of a potential, but are difficult to meet in general. Then, nonlinear elastic behavior is modeled in the framework of hyperelasticity by assuming and formulating directly that potential: the strain energy function [3, 5]. Traditionally, the models developed in this framework assume an analytical expression for the shape of the strain energy function, which is formulated in terms of a number of material parameters. These parameters are determined by fitting the predictions of the model at hand with experimental data through optimization algorithms. Hyperelastic models may be either phenomenological or structure-based, depending on whether or not the microstructure of the material constituents is explicitly accounted for in reproducing the overall macroscopic behavior of the material.

Arguably, phenomenological models are simpler and give more flexibility in reproducing the macroscopically observed behavior. A vast amount of phenomenological models has been proposed, each one with a different analytical proposal and frequently targeted at specific materials [11]. For isotropic, incompressible materials, the simplest Neohookean and the successful Ogden models [12, 11] are probably the most used phenomenological ones and are available in most finite element codes. The accuracy of this type of models depends on the number of terms employed in the analytical expressions, and thus, on the number of parameters. However, the determination of the material parameters is usually not trivial [13, 14], so a large amount of literature is dedicated just to that determination, see for example [15, 16]. A change of paradigm for phenomenological models has been given by Sussman and Bathe [17] in their model for isotropic, incompressible materials. Instead of using analytical functions, Sussman and Bathe used spline interpolations between values obtained from a numerical solution of the equilibrium equations by means of the Kearsley-Zapas formula [18]. We have extended these ideas to more complex materi-

als, e.g. compressible materials [19] and anisotropic materials [20], [21], as well as for unconventional materials [22]. We have coined this approach What-You-Prescribe is What-You-Get (WYPiWYG) hyperelasticity, the reason being that in contrast to formulations based on analytical functions, smooth experimental data are captured to any desired precision because equilibrium equations are numerically solved. Obviously, the resulting stored energies may be immediately used in the general loading conditions present at stress integration points during non-homogeneous finite element simulations [19], [23]. Relevant aspects of the novel approach are that no material parameters are employed and that noisy data are easily incorporated guaranteeing, when needed, some stability conditions [24]. Furthermore, the approach allows for capturing material behavior where other models fail, like in the cases of strong tension-compression asymmetry [25], where even a conventional small strain treatment results to be exceedingly complex, see e.g. [26, 27]. However, the phenomenological approach is arguably less satisfying from a scientific standpoint and requires more experimental data to give good results under general loading conditions. On the contrary, the second class of models, the microstructure-based models, use some information about the material which allows to obtain good predictions in general loading cases with substantially less experimental data and material parameters. In these models, a tensile test is often sufficient to characterize isotropic materials.

In the case of polymeric-like materials, their microstructure consists of a network of randomly oriented and coiled polymeric fibers which are gradually uncoiled when they are stretched. This fiber uncoiling process decreases entropy, increases forces and causes the macroscopic non-linear stress-strain behavior. The intermolecular interaction is neglected in the stored energy so that the stored elastic energy of a polymeric network can be obtained as the sum of the free energy of all the individual chains [2, 4]. The determination of the strain energy function of a single polymeric chain has been addressed through statistical mechanics, where a single fiber can be modeled as a worm-like chain or a freely-joined chain. In the worm-like chain approach, the chain is considered as a flexible and smooth beam with a continuous change of curvature due to thermal fluctuations [28]. The worm-like chain has been applied to reproduce soft tissues behavior [29] and biological remodeling [30, 31]. As in the case of freely-joined chains, the strain energy is entropy-based.

The freely-joined chain consists of N segments with a constant length l, so the contour length of the chain is $L = Nl$. These Khun segments are assumed rigid and randomly coiled but free to rotate without modifying the internal energy. Thus, the work of deformation of a single chain is considered to be given by the difference of the chain entropy between its unstretched and stretched configurations. Each chain

is characterized by the distance between the ends of the chain, r_{ch}, also called end-to-end distance. The maximum entropy s (possible configurations) is obtained for the isolated chain with $r_{ch} = 0$, whereas the initial length $r_0 = \sqrt{N}l$ is given by random walk statistics [2, 32]. This entropy decreases as the chain is stretched since the number of configurations that the chain can adopt is reduced. The configuration that a chain can achieve is mathematically expressed by a probability distribution function. When a chain is stretched in the range of large strains, instead of using the typical Gaussian distribution, a probability distribution function based on the inverse Langevin function, $\mathcal{L}^{-1}(r_{ch}/Nl) = y$, is adopted. This distribution accounts for the limit extensibility of the chain when $r_{ch} \to Nl$, in which case the entropy of the chain is minimum because it has only one possible configuration. A background on the statistical treatment of polymers can be found in the books from Treloar [2] and Mark and Erman [4].

In structure-based models, proposed material parameters are related to that microstructure; for example two typical parameters are N (number of segments of a typical chain) and n (chain density per unit volume). Thereafter, the spatial distribution of chains is accounted for by a simplified ideal layout. Earlier 3D models are the three-chain model [33] and the four chain model [34]. The material parameters in all cases are $G = nkT$ and N, where k is Boltzman's constant and T is the absolute temperature of the tests. However, the most popular model of this kind is the Arruda-Boyce [32] eight chain model (with more than 2000 cites, and available in most finite element programs), because using the same material constants obtained by fitting a macroscopic tensile test, the model predicts much better the behavior under a general case of deformation. The Arruda-Boyce model has also been extended to anisotropy, see [30] and [35, 36].

The purpose of the present paper is to show that WYPiWYG hyperelasticiy allows for a new approach also in microstructure-based hyperelasticity. In the phenomenological approach, WYPiWYG hyperelasticity eliminated the need for prescribing analytical functions and material parameters, leaving only the asumption of the employed reduced form, which in turn is actually determined by the available experimental data to give a well-posed material determination procedure. For the present microstructure-based approach, we show below that using WYPiWYG hyperelasticity, we can bypass the need to assume the probability density function of the chains and, hence, the material parameters. Furthermore, the assumptions regarding the fully entropic nature of elastic energy or the type of structural behavior of the single chain are not needed. With this proposal, the behavior of the average chain or fiber in the material is obtained by an inverse procedure from a single test (e.g. a tensile test) as a spline function. Then, the function may be used to derive

the stress-strain behavior of the solid under any arbitrary condition. The model gives better accuracy than the Arruda-Boyce model at the same computational cost. It may further use information of different tests to obtain an improved average chain behavior.

The WYPiWYG approach is mainly numerical, different from the analytical ones employed in the literature. Hence claims in this paper must be verified through a program. To this end, we include all code needed for the examples in this paper in the programming language Julia. Julia is still not as extended a Matlab, but it is an excellent freeware language for researchers working in computational mechanics, which typically employ fortran for speed and Matlab for testing (and specially for obtaining material parameters). Julia is easy to learn, with a visual structure very close to that of both fortran and Matlab, but solves the two-languaje paradigm: it is fast and productive. It is our believe that it will be soon the preferred programing language in computational mechanics.

The rest of the manuscript is organized as follows. First we summarize the relevant findings in chain-based models and we derive the relation between the average chain behavior and that of a deformed continuum without assuming a specific cell. Then we show that in fact, this relation is the same as that given by one of the eight chains of the Arruda-Boyce model, so the diagonals of their hexaedron result to be representative of the average chain. Then, following the WYPiWYG approach, instead of assuming the behavior of that average chain, we obtain it directly, in spline form, from macroscopic experimental data. We show that if we use the Arruda-Boyce model to generate pseudoexperimental data, we are able to reproduce exactly its behavior under any loading condition without employing their entropy-based relations and material parameters. Then we show the ability of the model to predict Treloar's tests in rubber materials [37] and explain the limitations regarding the equibiaxial test predictions. The Julia code is described briefly in the Appendix.

2. The chain behavior and its relation to the macroscopic behavior

For an isotropic incompressible material, given the stored energy function $\mathcal{W}\left(\lambda_1, \lambda_2, \lambda_3\right)$, the relation between the principal Cauchy stresses σ_i and the principal stretches λ_i is [12]

$$\sigma_i = -p + \lambda_i \frac{\partial \mathcal{W}\left(\lambda_1, \lambda_2, \lambda_3\right)}{\partial \lambda_i} \quad i = 1, 2, 3 \tag{1}$$

where p is the pressure-like Lagrange multiplier. The stored energy $\mathcal{W}$ of rubber-like materials, when considering Gaussian chain statistics and randomly oriented chains,

is given by the Neo-Hookean model [2]

$$\mathcal{W} = \tfrac{1}{2}G\left(I_1 - 3\right) \tag{2}$$

so

$$\sigma_1 - \sigma_2 = G\left(\lambda_1^2 - \lambda_2^2\right) \tag{3}$$

where $G = nkT$ is the constant (shear-like modulus) defined above and

$$I_1 = tr\left(\boldsymbol{C}\right) = tr\left(\boldsymbol{X}^T\boldsymbol{X}\right) = \lambda_1^2 + \lambda_2^2 + \lambda_3^2 \tag{4}$$

is the first invariant of the Cauchy-Green deformation tensor $\boldsymbol{C} = \boldsymbol{X}^T\boldsymbol{X}$, where $\boldsymbol{X}$ is the deformation gradient (we note that the deformation gradient is frequently denoted by $\boldsymbol{F}$, but we follow the notation of [1, 38] and of our previous works). We assume, as usual, that the material is incompressible, i.e. $\lambda_1\lambda_2\lambda_3 = 1$. As it is well known, Gaussian statistics do not account for the limiting extensibility of the chain. The limit length of a chain is given by $r_{ch} = L = Nl$. The stretch of the chain $\lambda_{ch} = r_{ch}/r_0$ then reaches a maximum value

$$\lambda_{lock} := \max\left(\lambda_{ch}\right) = \frac{L}{r_0} = \sqrt{N} \tag{5}$$

Using this fact, a better approximation for the probability distribution is given by the Langevin function. With this non-Gaussian treatment, the entropy of a chain is [2, 32]

$$s\left(r_{ch}\right) = k\ln\mathfrak{p}\left(r_{ch}\right) = k\left[c - N\left(\frac{r_{ch}}{Nl}y + \ln\frac{y}{\sinh y}\right)\right] \tag{6}$$

and the stored energy is

$$\mathcal{W} = -Ts = kTN\left(\frac{r_{ch}}{Nl}y + \ln\frac{y}{\sinh\left(y\right)}\right) - kcT \tag{7}$$

where $\mathfrak{p}\left(r_{ch}\right)$ is the probability density and $y = \mathcal{L}^{-1}\left(r_{ch}/Nl\right) = \mathcal{L}^{-1}\left(\lambda_{ch}r_0/Nl\right) = \mathcal{L}^{-1}\left(\lambda_{ch}/\sqrt{N}\right)$ is the inverse Langevin function, which analytical expression is unknown, but that can be obtained in an approximate manner from its inverse, the Langevin function

$$\mathcal{L}\left(y\right) = \coth y - \frac{1}{y} \Rightarrow \mathcal{L}^{-1}\left(\frac{\lambda_{ch}}{\sqrt{N}}\right) \simeq 3\frac{\lambda_{ch}}{\sqrt{N}} + \frac{9}{5}\left(\frac{\lambda_{ch}}{\sqrt{N}}\right)^2 + \dots \tag{8}$$

The tension force in the chain is obtained from the thermodynamic requirement

$$F_{ch}(r_{ch}) = -T\frac{ds(r_{ch})}{dr_{ch}} = \frac{kT}{l}\mathcal{L}^{-1}\left(\frac{r_{ch}}{Nl}\right) = \frac{kT}{l}\mathcal{L}^{-1}\left(\frac{\lambda_{ch}}{\sqrt{N}}\right) \tag{9}$$

and the nominal stress

$$P_{ch}(\lambda_{ch}) = -T\frac{ds(\lambda_{ch})}{d\lambda_{ch}} = F_{ch}(r_{ch})\frac{dr_{ch}}{d\lambda_{ch}} = \sqrt{N}l\ F_{ch}(r_{ch}) \tag{10}$$

For small values of r_{ch}/Nl, far away from locking, the Gaussian description is obtained, where

$$\mathcal{L}^{-1}\left(\frac{r_{ch}}{Nl}\right) \simeq 3\frac{r_{ch}}{Nl} = 3\frac{\lambda_{ch}}{\sqrt{N}} \tag{11}$$

and

$$F_{ch}(\lambda_{ch}) = 3\frac{kT}{l}\frac{\lambda_{ch}}{\sqrt{N}} \text{ so } P_{ch}(\lambda_{ch}) = 3kT\lambda_{ch} \tag{12}$$

but in the limit near the locking situation $\mathcal{L}^{-1}(1) \to \infty$, so $F_{ch}(\lambda_{lock}) \to \infty$ and by equilibrium $\lambda_{ch} \ngtr \lambda_{lock}$. Note that the Gaussian chain is linear in stretches.

The Langevin treatment of the chain behavior is theoretically very satisfying, but has some relevant limitations from a practical standpoint that should be beared in mind:

- Since there is no analytical expression for the computation of the inverse Langevin function, and the accuracy and efficiency in evaluating such function is extremely important at large strains [39], several approximants have been proposed, many of them in the last five years [40, 41, 42, 43, 44, 45]. With computational efficiency in mind, the most accurate approximant of the inverse Langevin function is our recent proposal, reaching near machine precision at the same cost of the most efficient approximants [46]. In this procedure, spline interpolations are employed as in WYPiWYG hyperelasticity.

- The Langevin statistical treatment is a remarkable advance over the Gaussian treatment because the former naturally captures the upturn behavior observed in experiments, an aspect which the latter cannot predict. However, this approach is neither exact; it represents an approximation of the actual probability distribution. It is accurate only for large enough values of N, say about $N = 25 \sim 50$, an important issue near the locking stretch (refer to Figs. 6.3 and 6.6 in [2]). Fitted values of N from macroscopic tests are often near this limit (see e.g. Figs 11 and 14 in [32]).
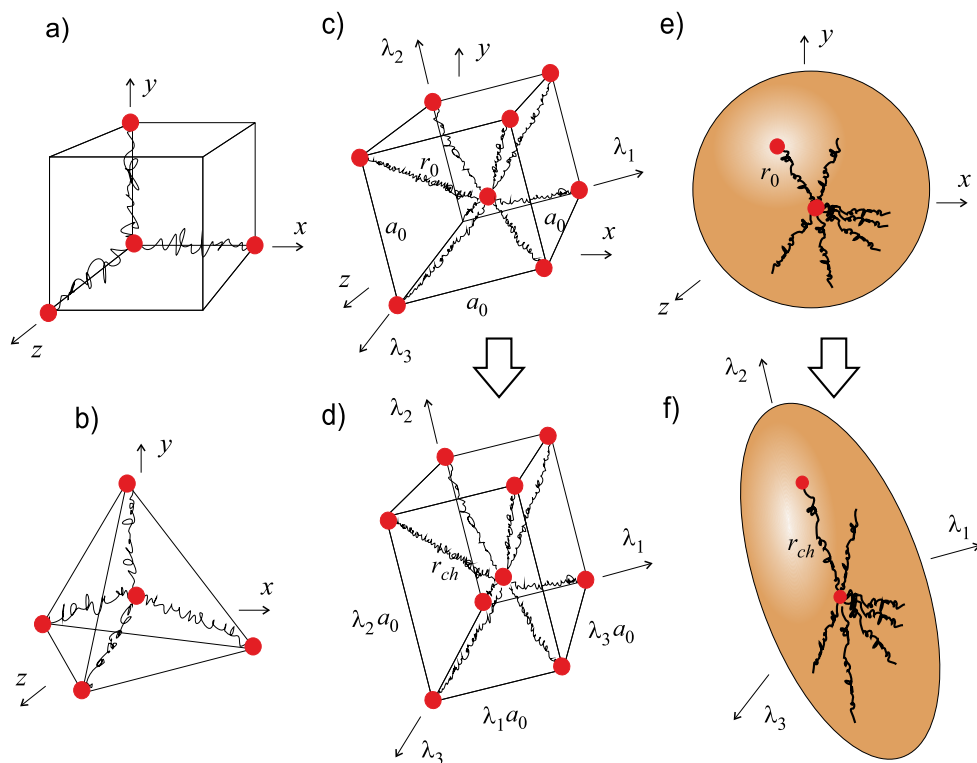
Figure 1: Network models. (a) Three chain model. (b) Four chain model. (c) Eight chain model in non-deformed configuration. (d) Eight chain model in deformed configuration. (e) Isotropic distribution of average-length chains; non-deformed configuration. (f) Isotropic distribution of average-length chains; deformed configuration.

- Stress-induced crystallization is important in some polymers [47], especially at large strains; see Fig. 1.9 in [2] and therein references. As noted in Ref. [48], in natural rubbers the (internal) energy component cannot be ignored for stretches larger than about 3.5 because of this phenomenon; see also discussions of Fig. 3.5 of [48], Figs 3 and 4 in [34] and references [49, 50], among others.

For the case of non-Gaussian models, the extension of the single chain behavior to compute the actual behavior of solids is performed through network models, as those shown in Fig. 1. The simplest model is the three-chain model, Fig 1a. In this model three chains are aligned with the coordinates of the problem (e.g. testing directions) or with the principal stretches (in later implementations) and the resulting

8

stress-strain behavior is [2, 51])

$$\sigma_i - \sigma_j = \frac{G}{3}\sqrt{N}\left[\lambda_i \mathcal{L}^{-1}\left(\frac{\lambda_i}{\sqrt{N}}\right) - \lambda_j \mathcal{L}^{-1}\left(\frac{\lambda_j}{\sqrt{N}}\right)\right] \tag{13}$$

which for the small values of Eq. (11) recovers the Neohookean relation Eq. (3). The four chain model, shown in Fig 1b, consists of four chains tying a free node to the vertices of a tetrahedron. It is usually considered as a non-affine model, where the central node is not tied to the continuum deformation imposed through the movement of the vertices, see [52]. The position of the central node is obtained solving the nonlinear equilibrium equations through iterative procedures. The consideration of non-affinity in this model results in substantialy different stress-strain behavior. However, as remarked by Arruda and Boyce [32] (see requirements in [51]), the model does not possess symmetry with respect to the principal stretch space. This requirement is related to the fundamental properties of isotropy and frame invariance [8]. Furthermore, these models did not capture correctly the difference in stress-stretch curves of the uniaxial and equibiaxial tests; see Figs. 12 and 13 of [32].

Because of these reasons, Arruda and Boyce proposed their eight chain model, see Fig. 1c. In their model, eight chains of length $r_0 = \sqrt{N}l$ radiate from a central node to the vertices of an hexaedron of dimension $a_0 = 2r_0/\sqrt{3}$. In order to guarantee the mentioned symmetry, they aligned the edges to the principal strain directions, see Figs. 1c and 1d. The vertices are subjected to the deformation of the continuum. All eight chains have the same stretch under any arbitrary deformation, so the model is affine (the internal node is always in equilibrium by the model symmetry respect to principal deformations). By geometric requirements, the stretch of each chain is directly related to the first invariant, see Fig. 1d

$$\lambda_{ch} = \frac{r_{ch}}{r_0} = \frac{\frac{1}{2}\sqrt{\lambda_1^2 a_0^2 + \lambda_2^2 a_0^2 + \lambda_3^2 a_0^2}}{\frac{1}{2}\sqrt{a_0^2 + a_0^2 + a_0^2}} = \sqrt{\frac{I_1}{3}} \tag{14}$$

Then, the strain energy function of the continuum is obtained from that of a single chain, Eq. (7), multiplying by the density of chains n. Substituting the chain stretch as a function of the macroscopic stretches, Eq. (14), and recalling that $G = nkT$, we obtain the relation

$$\frac{d\mathcal{W}}{d\lambda_i} = \frac{G}{3}\frac{\sqrt{N}}{\lambda_{ch}}\mathcal{L}^{-1}\left(\frac{\lambda_{ch}}{\sqrt{N}}\right)\lambda_i \tag{15}$$

9

which in turn, using Eq. (1), gives the following Cauchy stresses

$$\sigma_i - \sigma_j = \frac{G}{3}\frac{\sqrt{N}}{\lambda_{ch}}\mathcal{L}^{-1}\left(\frac{\lambda_{ch}}{\sqrt{N}}\right)(\lambda_i^2 - \lambda_j^2) \quad i \neq j \tag{16}$$

This model also recovers the Gaussian-based behavior as it is immediate to check using approximation Eq. (11) and comparing the result with Eq. (3). In contrast to the previous models, the macroscopic limit stretch is different for uniaxial and equibiaxial tests, but both are related to the same chain locking stretch. During uniaxial tests,

$$\frac{\lambda_{ch}}{\sqrt{N}} = \frac{1}{\sqrt{N}}\sqrt{\frac{\lambda^2 + 2/\lambda}{3}} \tag{17}$$

To get $\mathcal{L}^{-1}\left(\lambda_{ch}/\sqrt{N}\right) \to \infty$ we need $\lambda_{ch}/\sqrt{N} = 1$ and $\lambda^2 + 2/\lambda = 3N$ so for large λ we have a limit uniaxial stretch $\lambda_{\lim u} \simeq \sqrt{3N}$. In contrast, for equibiaxial tests

$$\frac{\lambda_{ch}}{\sqrt{N}} = \frac{1}{\sqrt{N}}\sqrt{\frac{2\lambda^2 + 1/\lambda}{3}} \tag{18}$$

so the limiting stretch is given by $2\lambda^2 + 1/\lambda = 3N$ which for large λ is $\lambda_{\lim e} \simeq \sqrt{3N/2}$. This gives the approximate relation for large stretches of

$$\lambda_{\lim e} \simeq \frac{1}{\sqrt{2}}\lambda_{\lim u} \tag{19}$$

For the pure shear test, $\lambda^2 + 1/\lambda = 3N$ and for large λ, $\lambda_{\min s} \simeq \sqrt{3N}$, which is the same limiting value obtained for uniaxial tests. This relation is qualitatively similar to the one observed in the experimental tests from Treloar, see Fig. 11 in [32]. Noteworthy, the three-chain and four-chain models do not predict such differences. Note for example that the three-chain Eq. (13) results in $\sigma_1 \to \infty$ when $\lambda_1/\sqrt{N} \simeq 1$, so the limiting stretch, for large strains is $\lambda_{\lim} \simeq \sqrt{N}$ for all cases (the locking stretch of a single chain). In fact, the values of N obtained from tensile tests for the three chain model are usually three times those of the Arruda-Boyce model, whereas the values of G (the small strain shear modulus) are coincident (compare for example Figs. 11 and 12 in [32]).

We mentioned that the Arruda-Boyce model is affine by construction, but a non-affine extension can also be established, albeit it implies an increment in the number of the model parameters [53, 54, 55]. The non-affinity has different relevance at different levels of deformation [2, 55]. The possibility of non-affinity is also considered

in the well known micro-sphere model, which is not based on the eight chain model but includes it as a particular case [56]. However, this model is substantially more expensive (needs numerical integration in the microsphere) and includes more parameters to improve experimental fitting, but the improvements are not substantial taking into account the significatively increased numerical effort [15]

To summarize the results explained in this section, we mention that the single chain behavior obtained from statistical mechanics has some approximations which may introduce relevant errors, and that the Arruda-Boyce model contains an adequate 3D structure of the chains layout, specially regarding the accountability of different locking strains for different tests, as observed in experiments.

3. Continuum behavior from the average chain behavior

The purpose of this section is to explain that, referring to quadratic strech measures, the average chain in a solid happens to be the same as that of the chains of the 8-chain model, so the Arruda-Boyce cell gives just a handy representation of the average deformation in the chains. However, considering that the behavior of all chains is given by that of the average chain, we also show that there is no need to make assumptions on the chain probability distribution to obtain the chain behavior. Instead of inferring chain parameters G and N from macroscopic data, we obtain the whole chain behavior from the same data in spline form through a simple inverse procedure. The resulting model is more accurate than the Arruda-Boyce model and the computational effort similar, since in the Arruda-Boyce model an accurate evaluation of the inverse Langevin function also needs a similar spline interpolation [46].

Consider a central node from which chains of average length r_0 radiate in any direction –see Fig. 1e. The undeformed length vector of a generic chain of average length is

$$\boldsymbol{r}_0 = r_0 \hat{\boldsymbol{r}}_0 = \begin{bmatrix} r_0 \sin\phi \cos\theta \\ r_0 \sin\phi \sin\theta \\ r_0 \cos\phi \end{bmatrix} \tag{20}$$

where ϕ and θ are the spherical angles. Then consider a deformation gradient $\boldsymbol{X}$ and $\boldsymbol{C} = \boldsymbol{X}^T \boldsymbol{X}$. The deformed length of each chain is given by

$$r_{ch}^2 (\lambda_1, \lambda_2, \lambda_3; \theta, \phi) = \boldsymbol{r}_0 \cdot \boldsymbol{C} \boldsymbol{r}_0 \tag{21}$$
$$= \tfrac{1}{4} r_0^2 \left[\lambda_1^2 \alpha (\theta, \phi) + \lambda_2^2 \beta (\theta, \phi) + \lambda_3^2 \gamma (\theta, \phi) \right] \tag{22}$$

where

11

$$\alpha\left(\theta,\phi\right) = 1 + \cos 2\theta - \cos 2\phi - \tfrac{1}{2}\cos\left(2\theta - 2\phi\right) - \tfrac{1}{2}\cos\left(2\theta + 2\phi\right) \qquad (23)$$

$$\beta\left(\theta,\phi\right) = 1 - \cos 2\theta - \cos 2\phi + \tfrac{1}{2}\cos\left(2\theta - 2\phi\right) + \tfrac{1}{2}\cos\left(2\theta + 2\phi\right) \qquad (24)$$

$$\gamma\left(\theta,\phi\right) = 2 + 2\cos 2\phi \qquad (25)$$

For given macroscopic stretches λ_i, the stretch is obtained from this expression as $\lambda_{ch}^2\left(\theta,\phi\right) = r_{ch}^2\left(\theta,\phi\right)/r_0^2$. Now considering a density of chains ρ in the sphere surface of average-chain length r_0, we have that, assuming an isotropic (constant) distribution, $\rho = const$, the average stretch of the chains may be computed as

$$\bar{\lambda}_{ch}^2 = \frac{\displaystyle\int_S r_{ch}^2\left(\theta,\phi\right)\rho dS}{\displaystyle\int_S r_0^2 \rho dS} \equiv \frac{1}{S}\int_S \frac{r_{ch}^2\left(\theta,\phi\right)}{r_0^2}dS$$

$$= \frac{1}{S}\int_0^{2\pi}\int_0^\pi \lambda_{ch}^2\left(\theta,\phi\right) r_0 \sin\phi d\phi d\theta \qquad (26)$$

Inserting the previous expressions in the integral, we end up with the result

$$\bar{\lambda}_{ch}^2 = \frac{\lambda_1^2 + \lambda_2^2 + \lambda_3^2}{3} = \frac{I_1}{3} \qquad (27)$$

If we compare this result with Eq. (14), we get to the conclusion that part of the success of the Arruda and Boyce model is due to the fact that the chains in their model of Fig. 1c have the same stretch as an average (representative) chain in the material.

In general, to keep the exposition intuitive and connected to the previous models, we may assume that the chain energy is entropy based, although this hypothesis is not needed as it will be apparent below. Then, the average chain has an entropy $s\left(\bar{\lambda}_{ch}\right)$, so the stored energy is

$$\mathcal{W}_{ch}\left(\bar{\lambda}_{ch}\right) = -Ts\left(\bar{\lambda}_{ch}\right) \qquad (28)$$

The nominal stress in the chain during an isothermal event is

$$P_{ch}\left(\bar{\lambda}_{ch}\right) = \frac{d\mathcal{W}_{ch}\left(\bar{\lambda}_{ch}\right)}{d\bar{\lambda}_{ch}} = -T\frac{ds\left(\bar{\lambda}_{ch}\right)}{d\bar{\lambda}_{ch}} \qquad (29)$$

12

A chain stability condition in the average chain may be set as $dP_{ch}\left(\bar{\lambda}_{ch}\right)/d\bar{\lambda}_{ch} = d^2\mathcal{W}_{ch}\left(\bar{\lambda}_{ch}\right)/d\bar{\lambda}_{ch}^2 > 0$, or $d^2s\left(\bar{\lambda}_{ch}\right)/d\bar{\lambda}_{ch}^2 < 0$; a condition which is met by the inverse Langevin function, see Eqs. (9) and (10). For a density of n chains per volume, the energy density is $\mathcal{W}\left(\lambda_1, \lambda_2, \lambda_3\right) = n\mathcal{W}_{ch}\left(\bar{\lambda}_{ch}\left(\lambda_1, \lambda_2, \lambda_3\right)\right)$, and the Cauchy stresses in the continuum are computed from Eq. (1)

$$
\begin{aligned}
\sigma_i - \sigma_j &= \lambda_i \frac{\partial \mathcal{W}\left(\lambda_1, \lambda_2, \lambda_3\right)}{\partial \lambda_i} - \lambda_j \frac{\partial \mathcal{W}\left(\lambda_1, \lambda_2, \lambda_3\right)}{\partial \lambda_j} \\
&= \left(\lambda_i \frac{\partial \bar{\lambda}_{ch}}{\partial \lambda_i} - \lambda_j \frac{\partial \bar{\lambda}_{ch}}{\partial \lambda_j}\right) nP_{ch}\left(\bar{\lambda}_{ch}\right)
\end{aligned}
\tag{30}
$$

where using Eq. (27)

$$
\frac{\partial \bar{\lambda}_{ch}}{\partial \lambda_i} = \frac{\lambda_i}{\bar{\lambda}_{ch}}
\tag{31}
$$

so

$$
\sigma_i - \sigma_j = f\left(\bar{\lambda}_{ch}\right)\left(\lambda_i^2 - \lambda_j^2\right) \quad \text{with } f\left(\bar{\lambda}_{ch}\right) = \frac{P_{nch}\left(\bar{\lambda}_{ch}\right)}{\bar{\lambda}_{ch}}
\tag{32}
$$

where $P_{nch}\left(\bar{\lambda}_{ch}\right) := nP_{ch}\left(\bar{\lambda}_{ch}\right)$. Note that this equation may be used in a general state of deformation, from which upon calculation of the principal stretches, we have $f(\bar{\lambda}_{ch}) = (\sigma_i - \sigma_j)/(\lambda_i^2 - \lambda_j^2)$. The function $f\left(\bar{\lambda}_{ch}\right)/n$ has the nature of a second Piola-Kirchhoff stress in a representative average chain. It is instructive to compare this expression with Eq. (16). Both equations are identical if we make the identification

$$
f\left(\bar{\lambda}_{ch}\right) = f_{AB}\left(\lambda_{ch}\right) := \frac{G}{3}\frac{\sqrt{N}}{\lambda_{ch}}\mathcal{L}^{-1}\left(\frac{\lambda_{ch}}{\sqrt{N}}\right)
\tag{33}
$$

Then, the present proposal can be viewed as an improved, more general formulation of the Arruda-Boyce model. However, we remark that we arrived at Eq. (32) without assuming a fictitious unit cell (as the hexaedron of the Arruda-Boyce model), but just considering the average chain in the material. Furthermore, we neither considered so far any chain behavior, nor configuration probability distribution. It is apparent from the previous derivations that none of them are needed, and furthermore, the same results would be obtained if a more general strain energy, not derived only from entropy, were considered. Then, the resulting Eq. (32) leaves a general form of the chain behavior though the function to be determined $f\left(\bar{\lambda}_{ch}\right)$. Whereas an analytical derivation from experimental tests is not simple, a spline-based representation, as performed in WYPiWYG hyperelasticity, is more straightforward, as we show below.

13

4. Numerical determination of the average-chain behavior

4.1. Inverse procedure to determine data for building $f(\lambda_{ch})$

Considering from now on $\bar{\lambda}_{ch} \equiv \lambda_{ch}$ as in the Arruda-Boyce model, the energy function proposed in the previous section gives

$$\sigma_i = -p + \lambda_i^2 f\left(\lambda_{ch}\right) \quad i = 1, 2, 3 \quad \text{with } f\left(\lambda_{ch}\right) = \frac{1}{\lambda_i} \frac{d\mathcal{W}}{d\lambda_i} \tag{34}$$

In the phenomenological models of WYPiWYG hyperelasticity, the first derivative of the energy function is obtained from the tensile and compression branches of uniaxial tests [14]. However, in this case, since the chains are always subjected to a tensile force, $f\left(\lambda_{ch}\right)$ can be determined by means of a single test. For example, if a tensile test is performed, $\sigma_2 = \sigma_3 = 0$ and $\sigma_1 \neq 0$. From the incompressibility condition and considering an isotropic behavior, we easily obtain that $\lambda_2 = \lambda_3 = 1/\sqrt{\lambda_1}$. After replacing these values in Eq. (32), the following relation between σ_1 and λ_1 is obtained

$$\sigma_1 = f\left(\lambda_{ch}\right)\left(\lambda_1^2 - \frac{1}{\lambda_1}\right) \tag{35}$$

which can also be expressed in nominal stress

$$P_1 = \frac{\sigma_1}{\lambda_1} = f\left(\lambda_{ch}\right)\left(\lambda_1 - \frac{1}{\lambda_1^2}\right) = \frac{\left(\lambda_1 - \dfrac{1}{\lambda_1^2}\right)}{\sqrt{\lambda_1^2 + \dfrac{2}{\lambda_1}}} P_{nch}\left(\lambda_{ch}\right) \tag{36}$$

where recall $P_{nch}\left(\lambda_{ch}\right) = \lambda_{ch} f\left(\lambda_{ch}\right)$.

Considering that the test consists on stretching the material in z steps, z pairs of data $\{\hat{\lambda}_{1i}^u, \hat{P}_{1i}^u\}$ are known, with $i = 1, ..., z$. The hat decoration emphasizes the fact of that the values are experimentally obtained and the superscript refers to the kind of test, namely u: uniaxial, b: equibiaxial, and s: pure shear. From every $\{\hat{\lambda}_{1i}^u, \hat{P}_{1i}^u\}$ the corresponding values of $f\left(\hat{\lambda}_{ch}^u\right)$ can be obtained from Eq. (36)

$$\hat{f}_i^u\left(\hat{\lambda}_{ch_i}^u\right) = \hat{P}_{1i}^u\left(\hat{\lambda}_{1i}^u - \frac{1}{\left(\hat{\lambda}_{1i}^u\right)^2}\right)^{-1} \tag{37}$$

Alternatively, we can also compute

$$P_{nch}\left(\hat{\lambda}_{ch_i}^u\right) = \hat{P}_{1i}^u \frac{\left(\hat{\lambda}_{1i}^u\right)^2}{\left(\hat{\lambda}_{1i}^u\right)^3 - 1} \sqrt{\frac{\left(\hat{\lambda}_{1i}^u\right)^3 + 2}{3\hat{\lambda}_{1i}^u}} \tag{38}$$

Each value of $\hat{f}_i^u$ is associated with a certain $\hat{\lambda}_{1i}^u$ and therefore with the corresponding value of $\hat{\lambda}_{ch_i}^u$ by Eq. (27). Thus, for every pair of data $\{\hat{\lambda}_{1i}^u, \hat{P}_{1i}^u\}$ given by the test, a pair of values $\{\hat{\lambda}_{ch_i}^u, \hat{f}_i^u\}$ are obtained through Eqs. (14) and (37) and accounting for the isotropic and incompressible conditions. Once all the z points, $\{\hat{\lambda}_{ch_i}^u, \hat{f}_i^u\}, i = 1, ..., z$ have been computed, they are interpolated by cubic splines so that $f(\lambda_{ch})$ is determined as a piecewise function of cubic polynomials. With this continuous $f(\lambda_{ch})$ function, the calculation of the Cauchy stress tensor is straightforward through Eq. (34) for any state of deformation, including the multiaxial one.

The calculation of the $f(\lambda_{ch})$ function should be independent of the test used in its determination, since it contains in essence the first derivative of the energy function, and this energy function is characteristic of the material and not of the kind of test performed for its determination. Thus the same $f(\lambda_{ch})$ function should be obtained if an equibiaxial or pure shear tests are employed.

In the case of an equibiaxial test, $P_1 = P_2 \neq 0$ and $P_3 = 0$, with $\lambda_1 = \lambda_2$ and $\lambda_3 = 1/\lambda_1^2$, considering an incompressible and isotropic material. For this case the discrete values of $f(\lambda_{ch})$ can be determined with —a similar expression applies for P_{nch}

$$\hat{f}_i^b\left(\hat{\lambda}_{ch_i}^b\right) = \hat{P}_{1i}^b \left(\hat{\lambda}_{1i}^b - \frac{1}{\left(\hat{\lambda}_{1i}^b\right)^5}\right)^{-1}$$

In the case of pure shear $\lambda_1 = \lambda$, $\lambda_2 = 1$, $\lambda_3 = 1/\lambda_1$, $P_3 = 0$ and $P_1 \neq 0$ are known. In this test, the values of $f(\lambda_{ch})$ for data $\{\hat{\lambda}_{1i}^{sh}, \hat{P}_{1i}^{sh}\}, i = 1, ..., z$ are

$$\hat{f}_i^s\left(\hat{\lambda}_{ch_i}^s\right) = \hat{P}_{1i}^s \left(\hat{\lambda}_{1i}^s - \frac{1}{1/\hat{\lambda}_{1i}^s}\right)^{-1}$$

To verify our procedure and to show that the Arruda-Boyce model can be reproduced just as a particular case, we have determined the function from "in-silico" tests performed on an Arruda-Boyce model with parameters $N = 26.5$ and $G = 0.27$. In Figure 2a the results for $\{\hat{\lambda}_{ch_i}, \hat{f}_i\}$ calculated from the virtual unaxial, equibiaxial
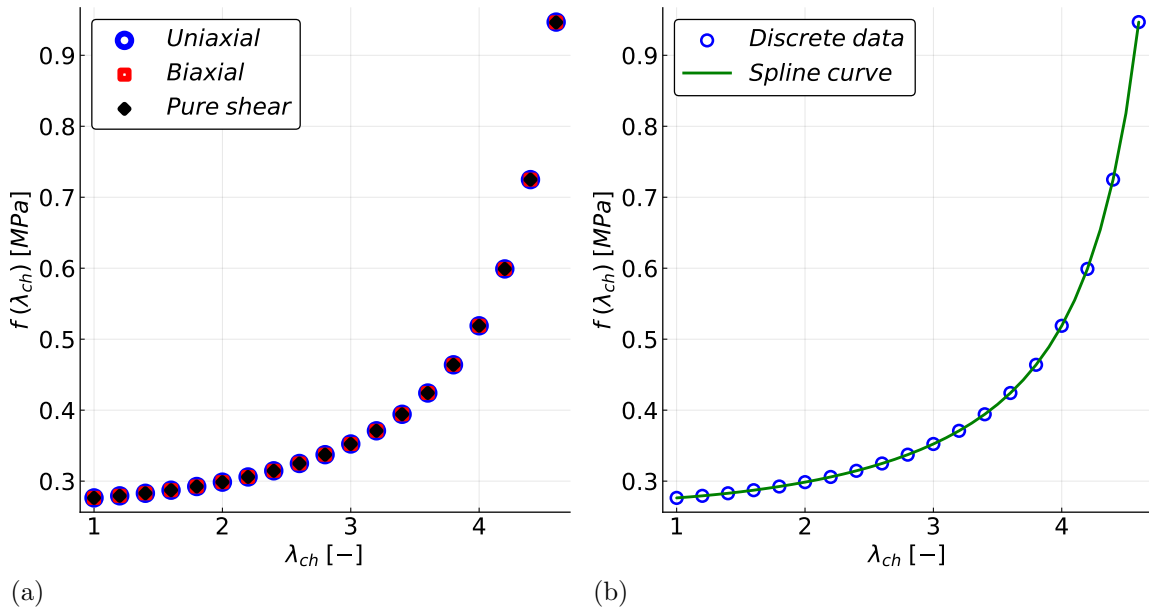
15

Figure 2: Numerical (inverse) determination of $f(\lambda_{ch})$ from "in-silico" tests performed over the Arruda-Boyce model (a) Discrete values obtained from uniaxial, equibiaxial and pure shear tests. (b) Cubic spline interpolation.

and pure shear tests are shown. It is clear that if $\hat{\lambda}^u_{ch_i} = \hat{\lambda}^b_{ch_i} = \hat{\lambda}^s_{ch_i}$ then we obtain the same average-chain response values $\hat{f}^u_i = \hat{f}^b_i = \hat{f}^s_i$ and then the spline interpolations for $f(\lambda_{ch})$ are also the same regardless of the test employed, Figure 2b. As above mentioned, this just means that, as it should be expected, the strain energy function and its derivatives are a unique characteristic of the material and not of the type of test.

Remarkably, it is easy to show that the obtained function from inverse analysis is also (numerically speaking) the same as that of the Arruda-Boyce model, i.e. Eq. (33) holds numerically at any arbitrary λ_{ch} value for the spline-based function $f(\lambda_{ch})$. And this holds to any desired precision: larger precision just means that we would need more spline pieces, *but this is also the case in the evaluation of the inverse Langevin function;* see [46]. Of course, this check on the function $f(\lambda_{ch})$ cannot be performed in a real material, because we cannot test the real average-chain behavior of the network in such cases.

4.2. Verification of the WYPiWYG model

In order to validate the procedure used to determine the average chain behavior, we assume that the Arruda-Boyce model is an actual material; i.e. we assume that

16

this model represents exactly the behavior of a given material. Then, using both the Arruda-Boyce model and our WYPiWYG model, we show in Fig. 3 that the predictions for a uniaxial, an equibiaxial and a pure shear test match exactly (numerically speaking), as it should be expected.

As a further interesting check, we show now that even if the material is under a general state of deformation, all the stress components are also identical. The importance of this example lies in the fact that during general, non-homogeneous finite element simulations of a material, each stress integration point is under a different deformation gradient. Then, if all the stresses match, not only the solution of both models will be the same, also the equilibrium iterations will match! [19]. Furthermore, the computational cost of both models is similar because of the approximants needed for an accurate evaluation of the Inverse Langevin function. Consider the following deformation gradient as a function of a scalar parameter γ (to facilitate plots)

$$\boldsymbol{X}(\gamma) = \begin{bmatrix} 1+\gamma & \gamma & 0 \\ 0 & 1+\gamma & 0 \\ 0 & 0 & (1+\gamma)^{-2} \end{bmatrix}$$

The same material parameters for the Arruda-Boyce model and also the same $f(\lambda_{ch})$ for the WYPiWYG model, calculated previously, are used in the present simulations. In Figure 4, the results of different components of the Cauchy stress tensor, calculated both using the Arruda-Boyce and the present WYPiWYG approach are depicted as a function of the parameter γ. Clearly, it is observed that, as expected, WYPiWYG hyperelasticity exactly mimics the eight chain model results.

5. Determination of $f(\lambda_{ch})$ from real experimental data

The obvious purpose of our approach is not to reproduce an analytical model but to obtain a model capable of reproducing the behavior of real materials. To show the applicability to real materials, we choose again Treloar's rubber, so the well-known tests by Treloar on that material are adopted [37]. These tests were also used by Arruda and Boyce to validate their eight chain model. Specifically, the authors calculated their model parameters fitting the predictions given by the eight chain model with the experimental uniaxial curve of the Treloar tests and then reproduced the other two tests, biaxial and pure shear, with the parameters calculated from the uniaxial one [32]. In our case, we determine functions $f(\lambda_{ch})$ from the three tests performed by Treloar.

The procedure is the same shown in Section 4.1. However, since Treloar's tests are real experiments over a real material, the data $\{\hat{\lambda}_{1i}^u, \hat{P}_{1i}^u\}$ obtained by Treloar
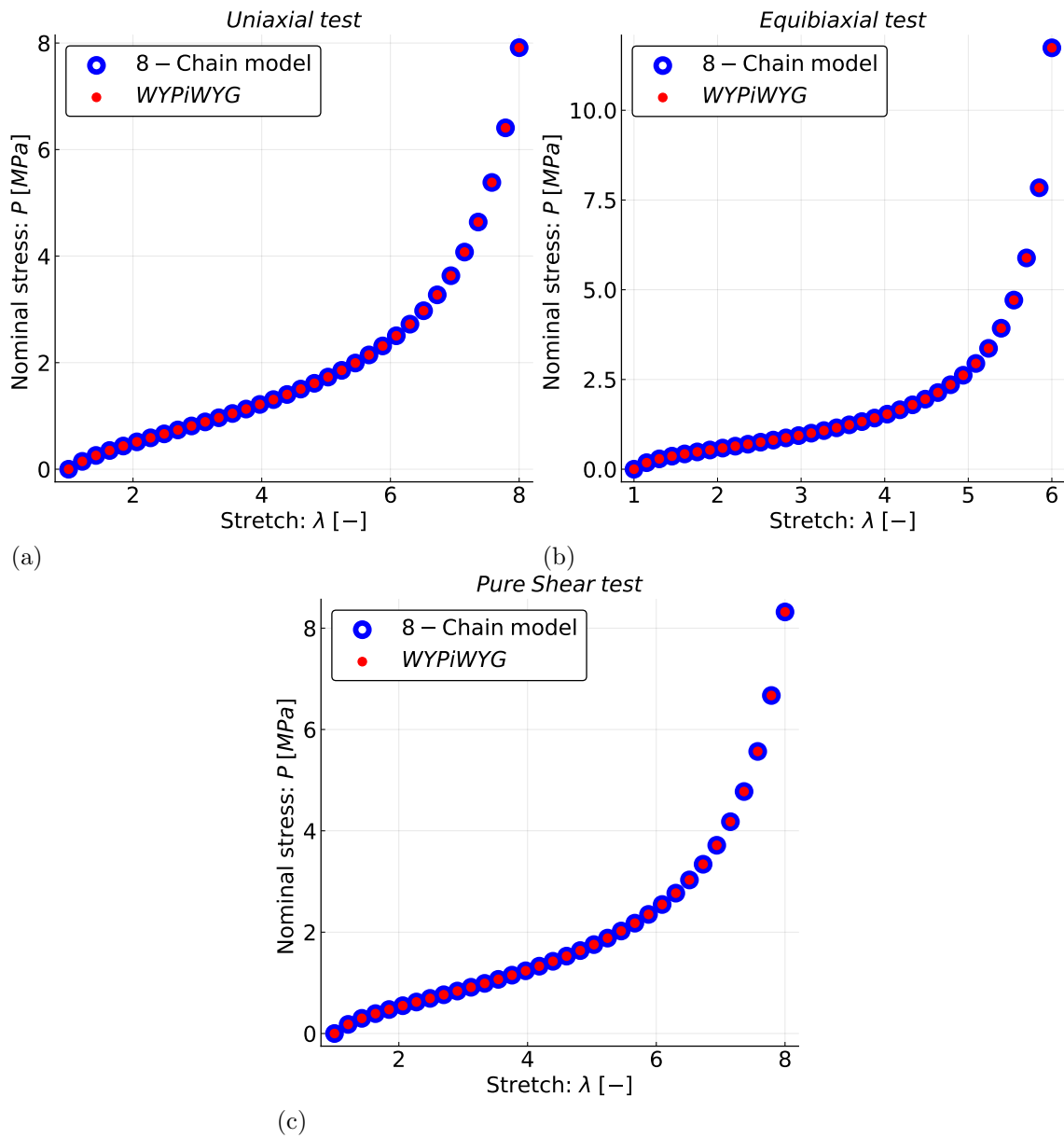
Figure 3: Results of the tests performed by means of the eight chain model and WYPiWYG model predictions. (a) Uniaxial test. (b) Equibiaxial test. (c) Pure shear test.
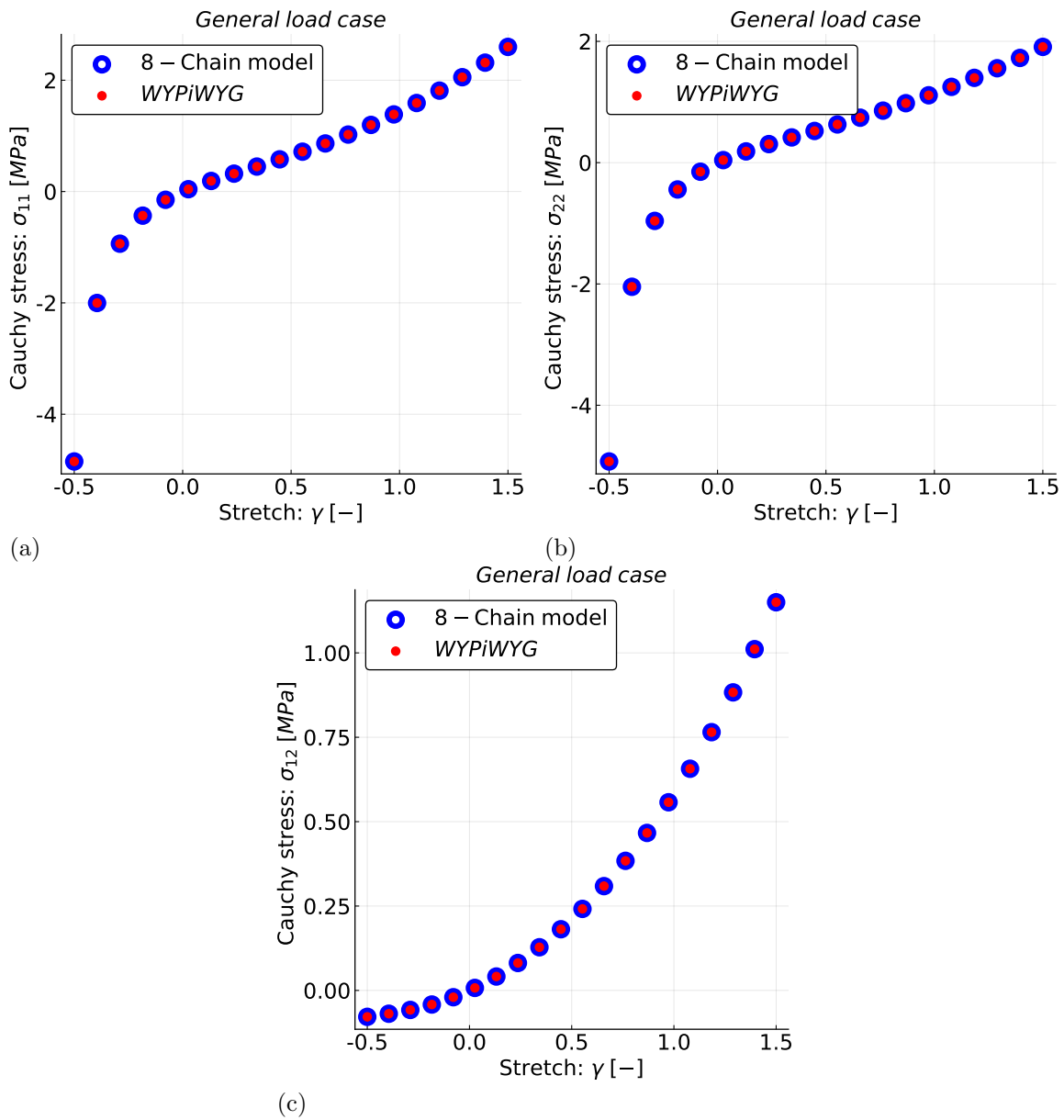
(a)

(b)

(c)

Figure 4: Cauchy stress tensor components for a general case of loading. Predictions given by the eight chain model and the WYPiWYG model using $N = 26.5$, $G = 0.27$ and the function $f(\lambda_{ch})$.

19

are not a smooth curve from which a realistic smooth $f(\lambda_{ch})$ may be determined. In order to obtain a smooth curve, a least squares approximation of the set of data $\{\hat{\lambda}_{chi}, \hat{f}_i\}$ is performed. In order to easily impose smoothness or stability conditions, we will use the periodic B-spline representation of cubic splines.

5.1. B-spline representation

B-splines are a mathematical tool widely used in the CAD industry. Based on Bézier curves, B-splines characterize and reproduce numerically smooth curves, surfaces and volumes [57]. B-splines of order k are defined through a set of basis function, $N_i^{(k)}$, and a set of vertices B_i which define a control polygon which plays the role of the B-spline hull. The basis functions are $k-1$ degree polynomials and are determined in a parameterized space from a knot vector. In our case B_i are the y coordinates of the vertices, but in general they can also be abscissae. The parametric form of a B-spline curve is

$$P(t) = \sum_{i=1}^{n} N_i^{(k)}(t) B_i = \boldsymbol{N}(t) \boldsymbol{B} \text{ with } t_{\min} \leq t_{\max} \text{ and } 2 \leq k \leq n \qquad (39)$$

where n is the number of vertices of the control polygon and the last term is the B-spline expressed in matrix notation. The basis functions have the partition of the unity property and are defined by the Cox-de Boor recursive formula. This formula determines every $N_i^{(k)}$ by linear interpolation of lower order basis functions. For more details see [57, 58].

Periodic B-splines are defined in a parametric space in which a periodic and uniform knot vector is defined by $t_i = i - 1$ with $i = 1, ..., k + n$. This knot vector gives periodic basis functions characterized by $N_{i-1}^{(k)}(t_{i-1}) = N_i^{(k)}(t_i) = N_{i+1}^{(k)}(t_{i+1})$, see Fig. 5. From this figure it is easy to deduce that the partition of unity condition is not obtained at the ends of the knot vector, specifically in the first and last $k-1$ segments so the usable parameter range is restricted to $k-1 \leq t \leq n+1$ and periodic B-splines span $m = n - k + 1$ segments. Since the periodic $N_i^{(k)}$ basis function is repeated in each segment, the corresponding basis functions can be re-parameterized to a coordinate $0 \leq \xi \leq 1$ in every curve element, and this same parameter may be used to normalize equispaced coordinates. Since every function spans k segments, the curve can be formulated

$$P_j(\xi) = \sum_{i=0}^{k-1} N_{i+1}(\xi) B_{j+i} \qquad (40)$$

where j subindex refers to the j-curve segment and the new parameter is $\xi =$

$(t - t_j) / (t_{j+1} - t_j) = (x - x_j) / (x_{j+1} - x_j)$. Note that every segment is labeled with the index of the first coordinate of the corresponding interval $[t_j, t_{j+1}]$.

For the periodic cubic B-splines ($k = 4$) that we use, we can write the matrix notation

$$P_j(\xi) = \sum_{i=0}^{k-1=3} N_{i+1}(\xi) B_{j+i} = \begin{bmatrix} N_1(\xi) & N_2(\xi) & N_3(\xi) & N_4(\xi) \end{bmatrix} \begin{bmatrix} B_j \\ B_{j+1} \\ B_{j+2} \\ B_{j+3} \end{bmatrix} \quad (41)$$

$$= \begin{bmatrix} \xi^3 & \xi^2 & \xi & 1 \end{bmatrix} \frac{1}{6} \begin{bmatrix} -1 & 3 & -3 & 1 \\ 3 & -6 & 3 & 0 \\ -3 & 0 & 3 & 0 \\ 1 & 4 & 1 & 0 \end{bmatrix} \begin{bmatrix} B_j \\ B_{j+1} \\ B_{j+2} \\ B_{j+3} \end{bmatrix} \quad (42)$$

The functions $N_i(\xi)$ are connected to the usual cubic splines using Eq. (42), so they are just a more convenient representation of the same curve. Some additional considerations are needed to obtain the partition of the unity in all the range of interest, which along the corresponding index numbering are summarized in Fig. 5.

5.2. Determination of a smoothed $f(\lambda_{ch})$ curve

In order to obtain a smoothed curve of $f(\lambda_{ch})$ a penalized least squares method is performed. For that, the vertices of the periodic B-splines that best fit the experimental results will be determined. In the problem at hand, the pairs of data $\{\hat{\lambda}_{1i}, \hat{P}_{1i}\}$ are taken from the corresponding Treloar's experiment test, with $i = 1, ..., z$. Then the corresponding $\hat{\lambda}_{chi}$ and $\hat{f}_i(\hat{\lambda}_{chi})$ are calculated, see Eqs. (27) and (36). These results can be arranged in a matrix form as $\hat{\boldsymbol{x}} = \left[\hat{\lambda}_{ch1}, ..., \hat{\lambda}_{chz}\right]^T$, and $\hat{\boldsymbol{y}}(\hat{\boldsymbol{x}}) = \left[\hat{f}_1, ..., \hat{f}_z\right]^T$.

The vertices of the control polygon that support the final continuous $f(\lambda_{ch})$ curve are determined as follows. Initially, the number of the vertices n and their abscisae are chosen within the interval $\boldsymbol{x}' = \left[\min\left(\hat{\lambda}_{ch1i}\right), \max\left(\hat{\lambda}_{ch1i}\right)\right]$. The goal is to calculate the corresponding ordinates of the B-spline vertices, $\boldsymbol{B} = [B_1, ..., B_n]^T$, that best fit the experimental data set $\{\hat{\lambda}_{chi}, \hat{f}_i\}$. It is worth noting that $\dim(\boldsymbol{B}) = n < z = \dim(\hat{\boldsymbol{x}})$. Once $\boldsymbol{B}$ has been obtained, the continuous $f(\lambda_{ch})$ is expressed as
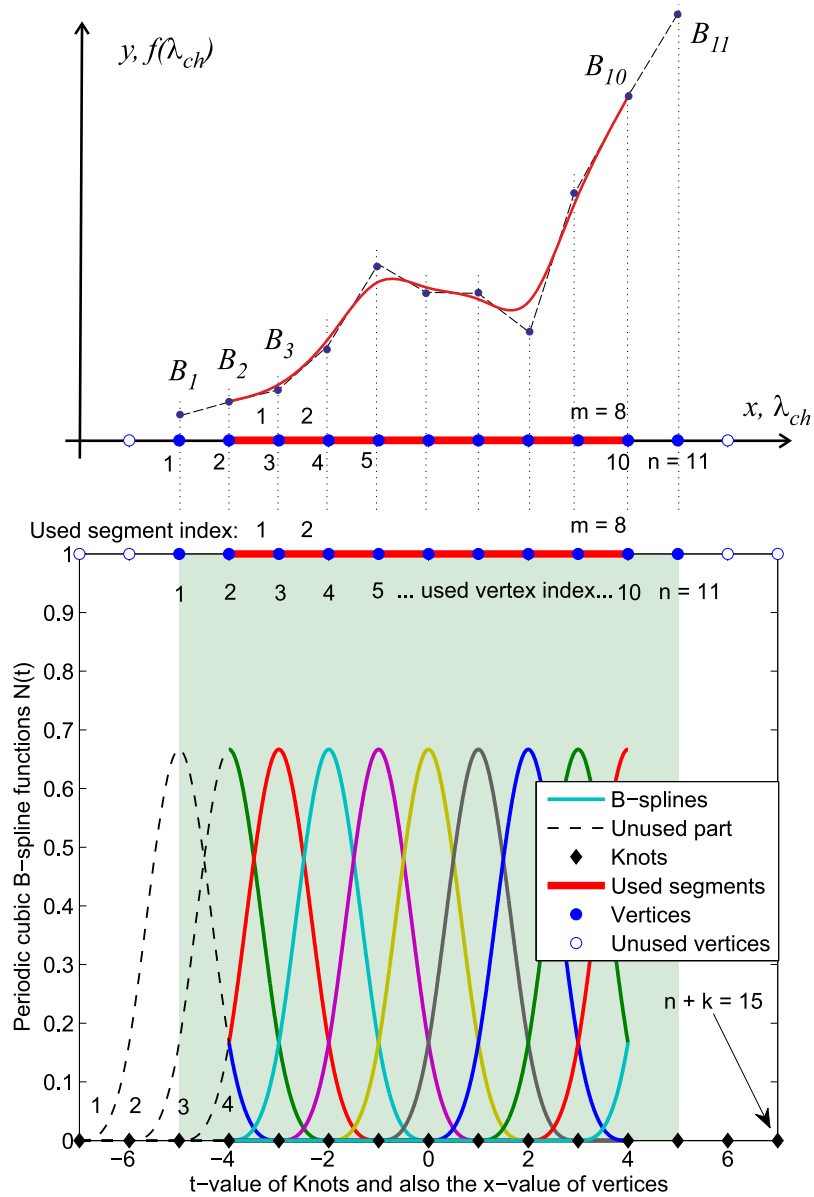
21

Figure 5: Periodic B-splines basis functions and B-spline representation of a curve [24]. Note that periodic representation is obtained using equally spaced knots, and to have partition of unity, two knots are discarded at each end. Spatially periodic functions are obtained with equal intervals. For a domain given by segments $m = 1, ..., 8$, two extra vertices must be calculated (so $n = 11$). This need is equivalent to the need for boundary conditions in the traditional cubic spline representation.

$$f\left(\lambda_{ch}\right) \equiv y\left(x\right) = \boldsymbol{N}\left(\boldsymbol{\xi}\left(x \in [x_j, x_{j+1}]\right)\right)\boldsymbol{B} \tag{43}$$

$$= \begin{bmatrix} \dots & 0 & N_1\left(\xi\right) & N_2\left(\xi\right) & N_3\left(\xi\right) & N_4\left(\xi\right) & 0 & \dots \end{bmatrix} \begin{bmatrix} \vdots \\ B_j \\ B_{j+1} \\ B_{j+2} \\ B_{j+3} \\ \vdots \end{bmatrix} \tag{44}$$

Since z values of $\hat{x}_i$ and $\hat{y}_i$ are available, Eq. (43) can be expressed in matrix form as

$$\boldsymbol{y}\left(\hat{\boldsymbol{x}}\right) = \boldsymbol{N}\left(\boldsymbol{\xi}\left(\hat{\boldsymbol{x}}\right)\right)\boldsymbol{B} \tag{45}$$

where $\boldsymbol{N}\left(\boldsymbol{\xi}\left(\hat{\boldsymbol{x}}\right)\right)$ is the matrix of basis function evaluations with dimensions $z \times n$, each row corresponding to a value of $\hat{x}_i$, and with just four contiguous non-zeros at the locations corresponding to the vertices of the segment at which $\hat{x}_i$ belongs. The leasts square objetive function to minimize is

$$g\left(\boldsymbol{B}\right) = \frac{1}{2}\left(\boldsymbol{y}\left(\hat{\boldsymbol{x}}\right) - \hat{\boldsymbol{y}}\left(\hat{\boldsymbol{x}}\right)\right)^T \boldsymbol{W}\left(\boldsymbol{y}\left(\hat{\boldsymbol{x}}\right) - \hat{\boldsymbol{y}}\left(\hat{\boldsymbol{x}}\right)\right) \tag{46}$$

where $\boldsymbol{W}$ is a $z \times z$ diagonal matrix containing weights values to give more importance to some data of the experimental test if considered. For example, we can enforce that the $f\left(\lambda_{ch}\right)$ curve passes through certain points. The least square minimization problem is

$$\min_{\boldsymbol{B}}\left\{g\left(\boldsymbol{B}\right)\right\} = \min_{\boldsymbol{B}}\left\{\frac{1}{2}\boldsymbol{B}^T\boldsymbol{N}^T\left(\hat{\boldsymbol{x}}\right)\boldsymbol{W}\boldsymbol{N}\left(\hat{\boldsymbol{x}}\right)\boldsymbol{B} - \boldsymbol{B}^T\boldsymbol{N}^T\left(\hat{\boldsymbol{x}}\right)\boldsymbol{W}\hat{\boldsymbol{y}}\left(\hat{\boldsymbol{x}}\right)\right\}$$

Choosing a number of vertices n less than the number of experimental data, gives already some smoothness. However, smoothness of the curve is better obtained by a penalty on the curvature. To do so, we adopt the simple and computationally efficient idea of Eilers and Marx [59]. They use the properties of the hull in controlling the curvature of the curve, so the penalty is performed using the following finite differences of the coefficients of adjacent B-splines

$$D_j^{(1)} = \frac{B_{j+1} - B_j}{x'_{j+1} - x\prime_j} = \frac{1}{h}\left(B_{j+1} - B_j\right) \tag{47}$$

$$D_j^{(2)} = \frac{D_{j+1}^{(1)} - D_j^{(1)}}{h} = \frac{1}{h^2}\left(B_{j+2} - 2B_{j+1} + B_j\right)$$

being $D_j^{(1)}$ and $D_j^{(2)}$ the approximations of the first and the second derivative respectively. Thus, the penalty function is defined as

$$\boldsymbol{B}^T \boldsymbol{D}^{(2)T} \boldsymbol{\Omega} \boldsymbol{D}^{(2)} \boldsymbol{B} \tag{48}$$

where $\boldsymbol{D}^{(2)}$ is a $[(n-2)\times n]$ matrix

$$\boldsymbol{D}^{(2)} = \frac{1}{h}\begin{bmatrix} 1 & -2 & 1 & 0 & 0 & 0 & 0 & ... & 0 \\ 0 & 1 & -2 & 1 & 0 & 0 & 0 & ... & 0 \\ 0 & 0 & 1 & -2 & 1 & 0 & 0 & ... & 0 \\ ... & ... & ... & ... & ... & ... & ... & ... & ... \\ 0 & 0 & ... & 0 & 0 & 1 & -2 & 1 & 0 \\ 0 & 0 & ... & ... & 0 & 0 & 1 & -2 & 1 \end{bmatrix} \tag{49}$$

and $\boldsymbol{\Omega}$ is a diagonal matrix that we introduce to play a similar role as the weights matrix $\boldsymbol{W}$ but with the second derivative. For example, to guarantee increasing curves, the terms of $\boldsymbol{\Omega}$ are increased at those vertices where $D_j^{(1)} < 0$. This increment is important, for example to guarantee stability of the obtained material. If we assume that the average chain gives an accurate description, then Eq. (9) requires that an increase in stretch of a chain should increase the tensile force and the nominal stress, Eq. (10). See discussion after Eq. (29). Then, stability in this sense can be obtained fitting $P_{nch}(\lambda_{ch})$ and requiring $dP_{nch}/d\lambda_{ch} > 0$. This requirement may be enforced increasing the values of Ω_j at the locations where $D_j^{(1)} < 0$ because overall, the curve fulfills the requirement. This smoothing procedure is similar to that given in Ref. [24], but since in this case only a test is involved and there is a clear micromechanical connection, the procedure results to be much simpler.

Finally, the (quadratic) objective function to be minimized is

$$\min_{\boldsymbol{B}} \left\{ \frac{1}{2}\boldsymbol{B}^T \boldsymbol{N}^T\left(\hat{\boldsymbol{x}}\right)\boldsymbol{W}\boldsymbol{N}\left(\hat{\boldsymbol{x}}\right)\boldsymbol{B} - \boldsymbol{B}^T\boldsymbol{N}^T\left(\hat{\boldsymbol{x}}\right)\boldsymbol{W}\hat{\boldsymbol{y}}\left(\hat{\boldsymbol{x}}\right) + \boldsymbol{B}^T\boldsymbol{D}^{(2)T}\boldsymbol{\Omega}\boldsymbol{D}^{(2)}\boldsymbol{B} \right\} \tag{50}$$

which results in a problem whose solution is immediately obtained solving a linear

system of equations; see [24]. With this method, a smoothed $f(\lambda_{ch})$ curve is obtained for the range encompassed by the test. This range does not usually include the full stretching of a chain, because experimental data does not either. In order to account for the full extensibility of the chain the following rational function is considered for $\lambda_{ch} \geq \max\left(\hat{\lambda}_{ch}\right)$

$$f_r(\lambda_{ch}) = \frac{a + b\lambda_{ch}}{c - \lambda_{ch}^2} \tag{51}$$

The constants a and b are determined enforcing $\mathcal{C}^1$ continuity at the end of the continous $f(\lambda_{ch})$ determined by Eq. (43). The last parameter, $c = \sqrt{\lambda_{lock}}$, is obtained considering an asymptote in the experimental curve $\left(\hat{\lambda}_{1i}, \hat{P}_{1i}\right)$ with the meaning of the value of the stretch $\lambda_{\lim 1} > \max\left(\hat{\lambda}_1\right)$, and therefore of $\lambda_{lock} > \max\left(\hat{\lambda}_{ch}\right)$, which produces the maximum extensibility of the chain. If $\max\left(\hat{\lambda}_1\right)$ is far away of the limit value, a good estimation for c is obtained visually from the discussion after Eq. (17). Otherwise, an automatic procedure is to enforce value and first and second derivatives at the continuity point (so all constants are determined directly from experimental data). In the code in the Appendix we leave this open.

5.3. Computational examples
5.3.1. Uniaxial test

In Figure 6a, the results corresponding to the determination of $f(\lambda_{ch})$ from the uniaxial test by Treloar are shown. Using this function, the results obtained for predicting uniaxial, biaxial and pure shear tests, in terms of the nominal stress, P_1, versus λ_1 stretch, are depicted in Figures 6b, 6c and 6d, respectively. It is shown that both uniaxial and shear tests are predicted quite well, whereas for the equibiaxial tests some larger discrepancies are observed.

5.3.2. Biaxial test

The $f(\lambda_{ch})$ curve obtained from the experimental results given by the equibiaxial test is depicted in 7a. The WYPiWYG predictions using this $f(\lambda_{ch})$ curve as well as the Treloar's experimental results are depicted in Figures 7b, 7c and 7d. Relative to the WYPiWYG predictions, the corresponding to the biaxial test improves greatly whereas for the uniaxial and pure shear tests, the model overestimates the nominal stress.

5.3.3. Pure shear test

The function $f(\lambda_{ch})$ determined by the experimental results of the pure shear test developed by Treolar is shown in 8a. The Treolar's experimental results for the
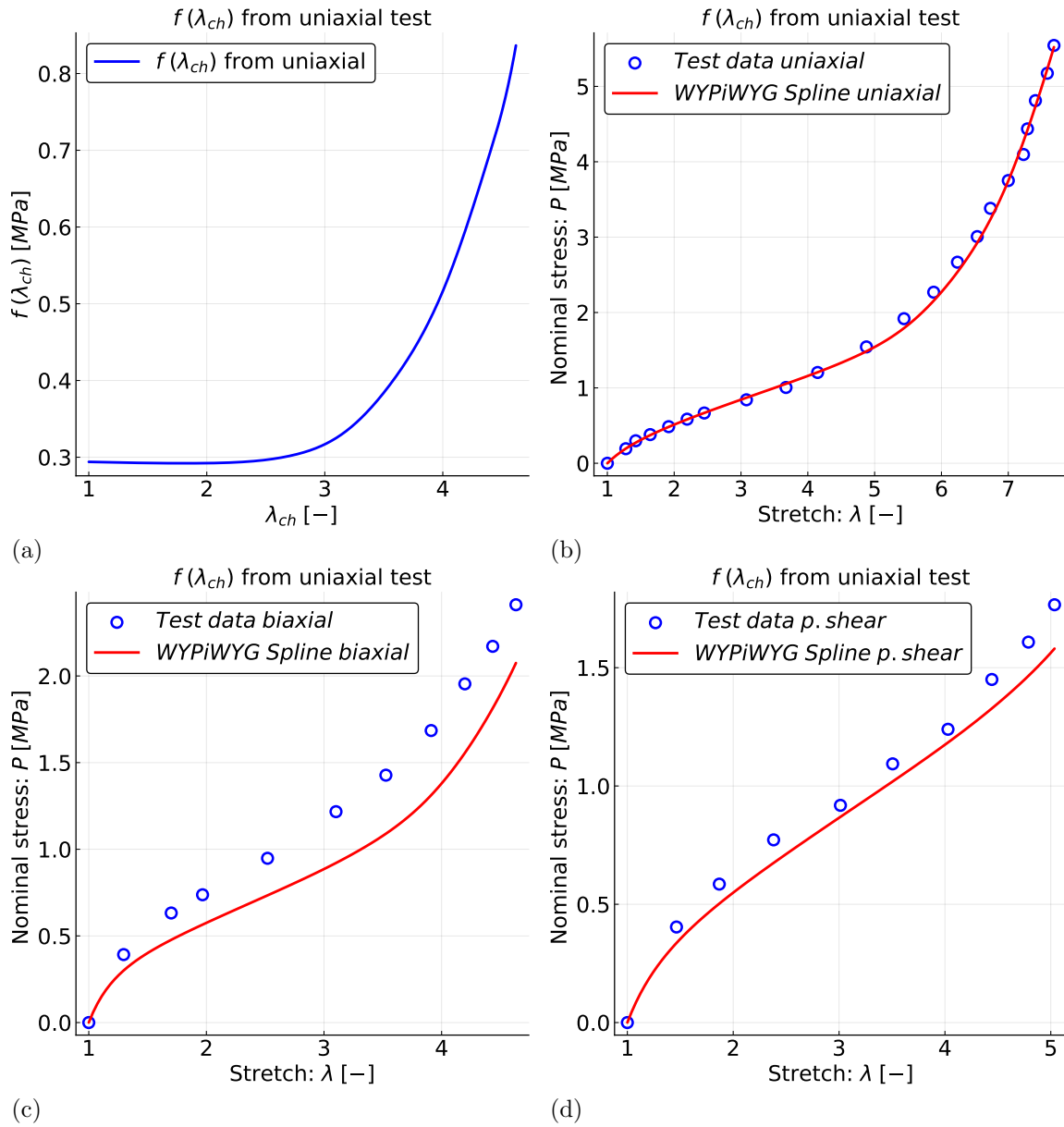
Figure 6: WYPiWYG model prediction, calculating $f(\lambda_{ch})$ for the uniaxial case, and experimental test results given by Treloar. (a) $f(\lambda_{ch})$ versus λ_{ch}. (b) Uniaxial test. (c) Equibiaxial test. (d) Pure shear test.
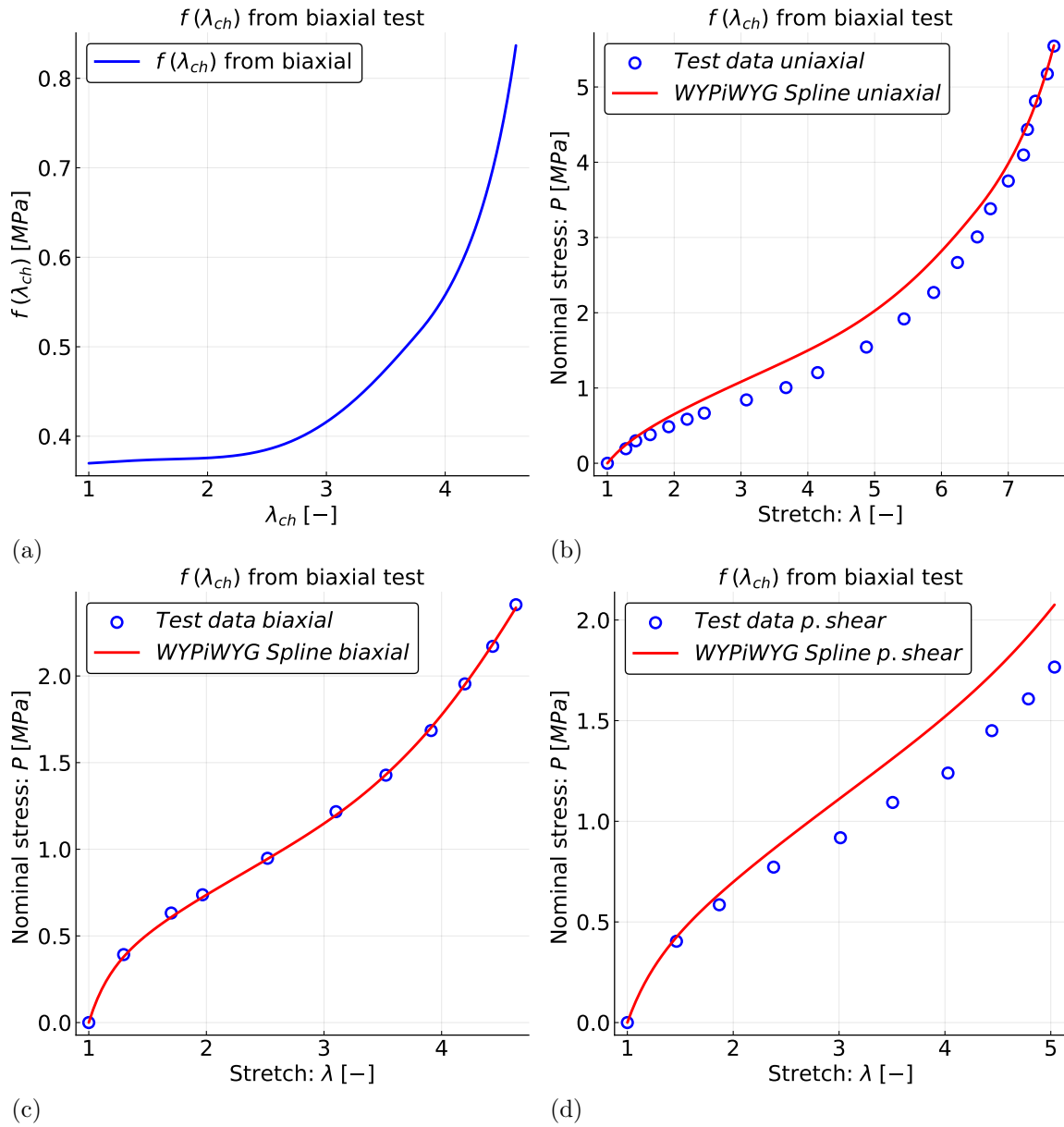
Figure 7: WYPiWYG model prediction, calculating $f\left(\lambda_{ch}\right)$ for the equibiaxial case, and experimental test results given by Treloar. (a)$f\left(\lambda_{ch}\right)$ versus λ_{ch}. (b) Uniaxial test. (c) Equibiaxial test. (d) Pure shear test.

27

three tests and the WYPiWYG predictions using the $f(\lambda_{ch})$ curve form pure shear are also shown in Figures 8b, 8c and 8d. The WYPiWIG model predictions are quite similar to the ones obtained with the $f(\lambda_{ch})$ calculated from the uniaxial test results, although the pure shear predictions are improved.

5.4. Discussion about the determination of the $f(\lambda_{ch})$ function

In Figure 9, the $f(\lambda_{ch})$ curves obtained from uniaxial, equibiaxial and pure shear experimental tests are depicted. Unlike Fig. 2, the three functions are not coincident. The difference is that in Fig. 2 the three $f(\lambda_{ch})$ functions were calculated from in-silico experiments over the 8-chain model, whereas in Figure 9 $f(\lambda_{ch})$ has been determined from real experimental test results. This explains why different predictions are obtained depending on the chosen test to determine $f(\lambda_{ch})$.

Since the strain energy function does not depend on the test but on the material, $f(\lambda_{ch})$ should be unique, so additional experimental data from additional tests should just increase the number of experimental points with which the unique function is determined. To do so we apply the same procedure of Section 5.2 but just considering simultaneously all the points of the three experimental tests developed by Treloar. In Figure 10a, the experimental data and the $f(\lambda_{ch})$ function calculated from all these data are depicted. The WYPiWYG predictions computed with this $f(\lambda_{ch})$ for the three tests are shown in Figs. 10b, 10c and 10d together with the corresponding experimental test results. As the predictions show, accurate results are obtained in the case of tensile and pure shear cases. In the equibiaxial test the model keeps underestimating the stress although the prediction is improved compared to the ones using $f(\lambda_{ch})$ only from uniaxial or pure shear results. Obviously we could increase the fitting on the equibiaxial tests by just increasing the weights W_i of those points. However, it is apparent from the data in Fig. 10a that a simultaneous fit of the three experiments is impossible using a model based just on average chain behavior. This observation is also common to the predictions of the Arruda-Boyce model. To understand the reasons for this discrepancy, we plot in Fig. 11 the ratios of the second and first invariants I_2/I_1 for the three tests. Noteworthy, the curve I_2/I_1 is remarkably different during the equibiaxial test, in which a clearly nonconstant evolution is observed. Both our model and the model from Arruda and Boyce use only the first invariant I_1. Then, the behavior of the material is characterized as a function of the first invariant, i.e. $\mathcal{W}(I_1)$, but a general expression for isotropic, incompressible materials is of the type $\mathcal{W}(I_1, I_2)$, where I_2 must come from non-average chain stretch terms, which are different in the tensile and equibiaxial tests. The experiments of Rivlin and Sounders and Obata et al (see discussion in Chapter 10 of [2]) show that the second invariant may have a relevant contribution. In our model, as well as in the
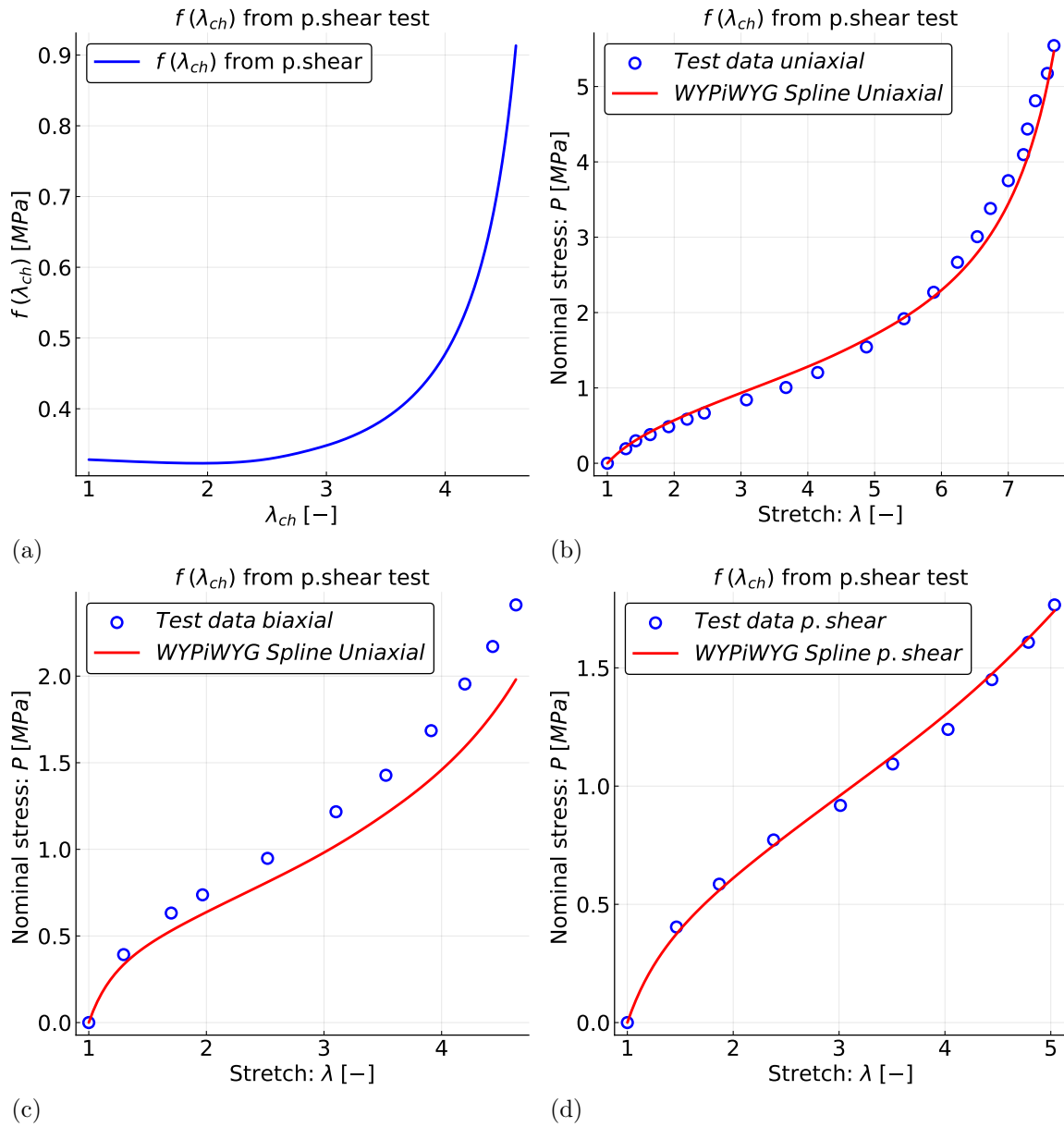
28

Figure 8: WYPiWYG model prediction, calculating $f(\lambda_{ch})$ for the pure shear case, and experimental test results given by Treloar. (a)$f(\lambda_{ch})$ versus λ_{ch}. (b) Uniaxial test. (c) Equibiaxial test. (d) Pure shear test.
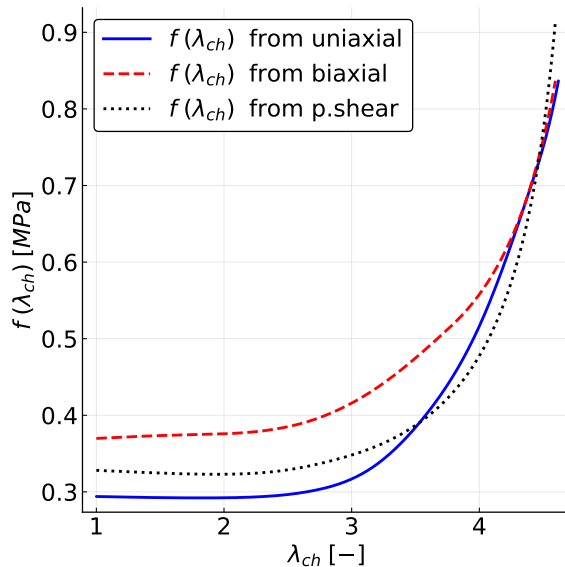
Figure 9: The three $f(\lambda_{ch})$ functions calculated from uniaxial, equibiaxial and pure shear experimental results.

Arruda-Boyce model, that contribution may be embed in that of the first invariant if the relation between both invariants remains approximately constant, but not when there are large variations of I_2/I_1 because then, two independent variables are needed. As a summary, the deviations of the predictions shown for the equibiaxial test (or conversely in the other two tests) may come from a relative change in the contributions of the first and second invariants in the stored energy, which cannot be accounted for by a model using a single independent variable (name it average-chain stretch or first invariant).

6. Conclusions

In this paper we present an inverse procedure to determine the function characterizing the behavior of an average chain in polymers. This function is then employed in a microstructure-based WYPiWYG hyperelastic model. In characterizing the chain behavior, we do not employ any assumed probability distribution function (or even an entropic origin of such behavior). However, the average-chain stretch of the model results to be the same as the stretch present in each of the chains of the 8-chain model from Arruda and Boyce. The practical importance of the model is that it can determine, from micromechanics, the stored energy of a solid when one single test is
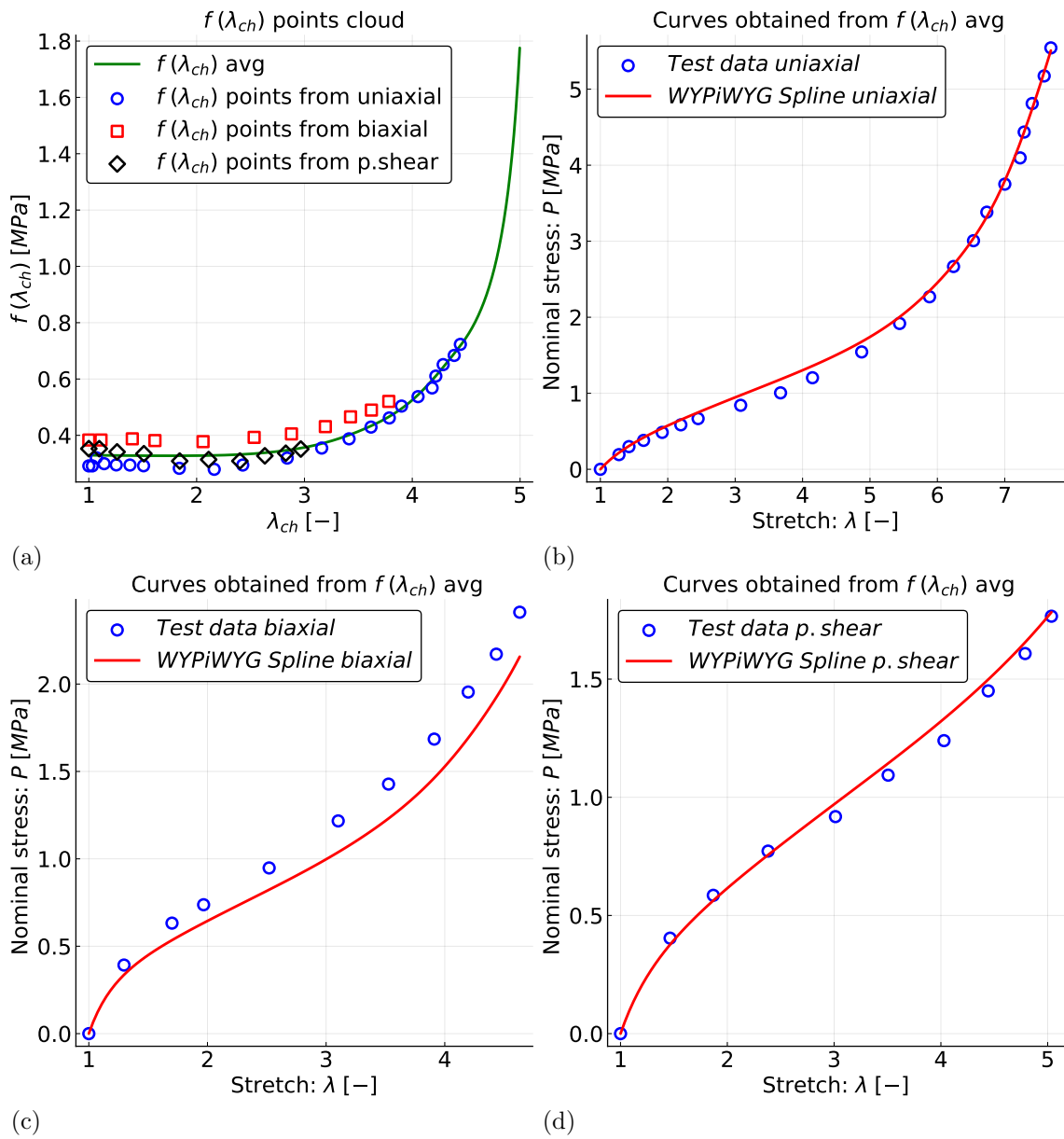
30

Figure 10: WYPiWYG model predictions using a $f(\lambda_{ch})$ function averaged from all the experimental test data given by Treloar. (a)$f(\lambda_{ch})$ versus λ_{ch}. (b) Uniaxial test. (c) Equibiaxial test. (d) Pure shear test.
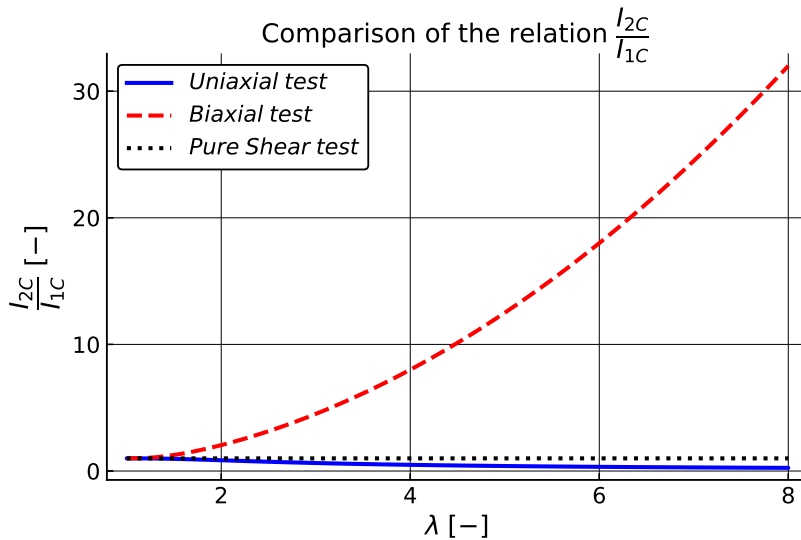
Figure 11: Evolution of the ratio I_2/I_1 of the invariants of $\boldsymbol{C}$ against the stretch of the experiment during uniaxial, equibiaxial and pure shear.

available. Its implementation in a finite element code is straightforward and its handling at user level is easy and simple. If more tests are available, the experimental data from those tests may be immediately used to increase the information for obtaining the chain behavior. The model is also capable of replicating the behavior of the Arruda-Boyce model under any loading condition just employing its macroscopic behavior during a tensile test. However, the proposed model is more flexible than the Arruda-Boyce model in fitting experimental results at the same computational cost than their model.

An aspect in common also with the Arruda-Boyce model is that if both models are characterized using a tensile test, the predictions for the equibiaxial test are not as accurate. The reason seems to be that both models result in stored energy functions of the first invariant. The incorporation of the second invariant through non-averaged micromechanical terms is ongoing work.

Finally, we include the code in Julia for the model and scripts to obtain most figures of the paper. These functions may be used also in future nonlinear finite element programs developed in the promising language Julia.

Acknowledgements

References

[1] K.-J. Bathe, Finite element procedures, 2nd Ed., Klaus-Jürgen Bathe, 2014.

[2] L. R. G. Treloar, The physics of rubber elasticity, Oxford University Press, USA, 1975.

[3] J. S. Bergstrom, Mechanics of solid polymers: theory and computational modeling, William Andrew, 2015.

[4] J. E. Mark, B. Erman, Rubberlike elasticity: a molecular primer, Cambridge University Press, 2007.

[5] J. M. Benítez, F. J. Montáns, The mechanical behavior of skin: Structures and models for the finite element analysis, Computers & Structures 190 (2017) 75–107.

[6] G. Gabriel, K. Bathe, Some computational issues in large strain elasto-plastic analysis, Computers & Structures 56 (2-3) (1995) 249–267.

[7] M. Kojić, K.-J. Bathe, Studies of finite element procedures—stress solution of a closed elastic strain path with stretching and shearing using the updated Lagrangian Jaumann formulation, Computers & Structures 26 (1-2) (1987) 175–179.

[8] C. Truesdell, W. Noll, The Non-linear Field Theories of Mechanics (revised ed.), Springer, 2004.

[9] B. Bernstein, Hypo-elasticity and elasticity, Archive for Rational Mechanics and Analysis 6 (1) (1960) 89–104.

[10] B. Bernstein, Relations between hypo-elasticity and elasticity, Transactions of the Society of Rheology 4 (1) (1960) 23–28.

[11] K. Volokh, Mechanics of soft materials, Springer, 2016.

[12] R. W. Ogden, Non-linear elastic deformations, Courier Corporation (Dover), 1997.

[13] R. Ogden, G. Saccomandi, I. Sgura, Fitting hyperelastic models to experimental data, Computational Mechanics 34 (6) (2004) 484–502.

[14] M. Latorre, E. De Rosa, F. J. Montáns, Understanding the need of the compression branch to characterize hyperelastic materials, International Journal of Non-Linear Mechanics 89 (2017) 14–24.

[15] P. Steinmann, M. Hossain, G. Possart, Hyperelastic models for rubber-like materials: consistent tangent operators and suitability for Treloars data, Archive of Applied Mechanics 82 (9) (2012) 1183–1217.

[16] M. Hossain, P. Steinmann, More hyperelastic models for rubber-like materials: consistent tangent operators and comparative study, Journal of the Mechanical Behavior of Materials 22 (1-2) (2013) 27–50.

[17] T. Sussman, K.-J. Bathe, A model of incompressible isotropic hyperelastic material behavior using spline interpolations of tension–compression test data, Communications in Numerical Methods in Engineering 25 (1) (2009) 53–63.

[18] E. Kearsley, L. Zapas, Some methods of measurement of an elastic strain-energy function of the valanis-landel type, Journal of Rheology 24 (4) (1980) 483–500.

[19] J. Crespo, M. Latorre, F. J. Montáns, WYPIWYG hyperelasticity for isotropic, compressible materials, Computational Mechanics 59 (1) (2017) 73–92.

[20] M. Latorre, F. J. Montáns, Extension of the Sussman–Bathe spline-based hyperelastic model to incompressible transversely isotropic materials, Computers & Structures 122 (2013) 13–26.

[21] M. Latorre, F. J. Montáns, What-you-prescribe-is-what-you-get orthotropic hyperelasticity, Computational Mechanics 53 (6) (2014) 1279–1298.

[22] J. Crespo, F. J. Montáns, A continuum approach for the large strain finite element analysis of auxetic materials, International Journal of Mechanical Sciences 135 (2018) 441–457.

[23] E. De Rosa, M. Latorre, F. J. Montáns, Capturing anisotropic constitutive models with WYPiWYG hyperelasticity; and on consistency with the infinitesimal theory at all deformation levels, International Journal of Non-Linear Mechanics 96 (2017) 75–92.

[24] M. Latorre, F. J. Montáns, Experimental data reduction for hyperelasticity, Computers & Structures, in pressdoi:10.1016/j.compstruc.2018.02.011.

[25] M. Latorre, M. Mohammadkhah, C. K. Simms, F. J. Montans, A continuum model for tension-compression asymmetry in skeletal muscle, Journal of the Mechanical Behavior of Biomedical Materials 77 (2018) 455–460.

[26] Z. Du, X. Guo, Variational principles and the related bounding theorems for bi-modulus materials, Journal of the Mechanics and Physics of Solids 73 (2014) 183–211.

[27] Z. Du, Y. Zhang, W. Zhang, X. Guo, A new computational framework for materials with different mechanical responses in tension and compression and its applications, International Journal of Solids and Structures 100 (2016) 54–73.

[28] R. W. Ogden, G. Saccomandi, I. Sgura, On worm-like chain models within the three-dimensional continuum mechanics framework, in: Proceedings of the Royal Society of London A: Mathematical, Physical and Engineering Sciences, Vol. 462, The Royal Society, 2006, pp. 749–768.

[29] G. Limbert, A mesostructurally-based anisotropic continuum model for biological soft tissues—decoupled invariant formulation, Journal of the Mechanical Behavior of Biomedical Materials 4 (8) (2011) 1637–1657.

[30] E. Kuhl, K. Garikipati, E. M. Arruda, K. Grosh, Remodeling of biological tissue: mechanically induced reorientation of a transversely isotropic chain network, Journal of the Mechanics and Physics of Solids 53 (7) (2005) 1552–1573.

[31] E. Kuhl, G. A. Holzapfel, A continuum model for remodeling in living structures, Journal of Materials Science 42 (21) (2007) 8811–8823.

[32] E. M. Arruda, M. C. Boyce, A three-dimensional constitutive model for the large stretch behavior of rubber elastic materials, Journal of the Mechanics and Physics of Solids 41 (2) (1993) 389–412.

[33] P. J. Flory, J. Rehner Jr, Statistical mechanics of cross-linked polymer networks i. rubberlike elasticity, The Journal of Chemical Physics 11 (11) (1943) 512–520.

[34] H. M. James, E. Guth, Theory of the elastic properties of rubber, The Journal of Chemical Physics 11 (10) (1943) 455–481.

[35] J. E. Bischoff, E. M. Arruda, K. Grosh, Finite element simulations of orthotropic hyperelasticity, Finite Elements in Analysis and Design 38 (10) (2002) 983–998.

[36] J. Bischoff, E. Arruda, K. Grosh, A microstructurally based orthotropic hyperelastic constitutive law, Journal of Applied Mechanics 69 (5) (2002) 570–579.

[37] L. Treloar, Stress-strain data for vulcanized rubber under various types of deformation, Rubber Chemistry and Technology 17 (4) (1944) 813–825.

[38] E. N. Dvorkin, M. B. Goldschmit, Nonlinear Continua, Springer-Verlag, Berlin, 2005.

[39] A. Ammar, Effect of the inverse Langevin approximation on the solution of the Fokker–Planck equation of non-linear dilute polymer, Journal of Non-Newtonian Fluid Mechanics 231 (2016) 1–5.

[40] A. N. Nguessong, T. Beda, F. Peyraut, A new based error approach to approximate the inverse Langevin function, Rheologica Acta 53 (8) (2014) 585–591.

[41] M. Kröger, Simple, admissible, and accurate approximants of the inverse Langevin and Brillouin functions, relevant for strong polymer deformations and flows, Journal of Non-Newtonian Fluid Mechanics 223 (2015) 77–87.

[42] M. Itskov, R. Dargazany, K. Hörnes, Taylor expansion of the inverse function with application to the Langevin function, Mathematics and Mechanics of Solids 17 (7) (2012) 693–701.

[43] R. Jedynak, New facts concerning the approximation of the inverse Langevin function, Journal of Non-Newtonian Fluid Mechanics 249 (2017) 8–25.

[44] B. C. Marchi, E. M. Arruda, An error-minimizing approach to inverse Langevin approximations, Rheologica Acta 54 (11-12) (2015) 887–902.

[45] E. Darabi, M. Itskov, A simple and accurate approximation of the inverse Langevin function, Rheologica Acta 54 (5) (2015) 455–459.

[46] J. M. Benitez, F. J. Montáns, A simple and efficient numerical procedure to compute the inverse langevin function with high accuracy, Journal of Non–Newtonian Fluids Mechanics 261 (2018) 153–163.

[47] I. Rao, K. Rajagopal, A study of strain-induced crystallization of polymers, International Journal of Solids and Structures 38 (6-7) (2001) 1149–1167.

[48] E. Riande, R. Díaz-Calleja, M. G. Prolongo, R. M. Masegosa, C. Salom, Polymer Viscoelasticity. Stress and Strain in Practice, Marcel Dekker, 2000.

[49] A. Williams, Polymer Science and Engineering, Prentice-Hall, New Jersey, 1970.

[50] R. Anthony, R. Caston, E. Guth, Equations of state for natural and synthetic rubber-like materials, Journal of Physics and Chemistry 46 (8) (1942) 826–840.

[51] M. C. Wang, E. Guth, Statistical theory of networks of non-gaussian flexible chains, The Journal of Chemical Physics 20 (7) (1952) 1144–1157.

[52] F. Aldakheel, C. Miehe, Coupled thermomechanical response of gradient plasticity, International Journal of Plasticity 91 (2017) 1–24.

[53] M. Kroon, An 8-chain model for rubber-like materials accounting for non-affine chain deformations and topological constraints, Journal of Elasticity 102 (2) (2011) 99–116.

[54] A. R. Cioroianu, E. M. Spiesz, C. Storm, An improved non-affine arruda-boyce type constitutive model for collagen networks, Biophysical Journal 104 (2) (2013) 511a.

[55] A. R. Cioroianu, E. M. Spiesz, C. Storm, Disorder, pre-stress and non-affinity in polymer 8-chain models, Journal of the Mechanics and Physics of Solids 89 (2016) 110–125.

[56] C. Miehe, S. Göktepe, F. Lulei, A micro-macro approach to rubber-like materials—part I: the non-affine micro-sphere model of rubber elasticity, Journal of the Mechanics and Physics of Solids 52 (11) (2004) 2617–2660.

[57] D. F. Rogers, An introduction to NURBS: with historical perspective, Elsevier, 2000.

[58] C. de BOOR, A practical guide to splines, Springer Verlag., 1978.

[59] P. H. Eilers, B. D. Marx, Flexible smoothing with b-splines and penalties, Statistical Science (1996) 89–102.

Appendix A. Description of the Julia code for the model and for simulations

In this Appendix we give a brief description of the files included as additional material. The code has been verified in Julia version 1.0.1 (2018-09-29).

The compressed file given with the paper contains two folders (`Pictures` and `TesData`), two Julia scripts (`arruda_wypiwyg.jl` and `arruda_wypiwyg_treloar.jl`) and two modules (`MathematicsToolsWYPIWYG.jl` and `WYPIWYGabTools.jl`). The modules contain all the functions required for the execution of the scripts.

When the script `arruda_wypiwyg.jl` is executed all the figures collected in Section 4.2 are generated and saved in a subfolder of the `Pictures` folder. When the script `arruda_wypiwyg_treloar.jl` is executed all the figures of Section 5.3 are generated and saved in another subfolder of the `Pictures` folder. The experimental data used for Treloar's tests [37] are available in the folder `TestData` in `.txt` format.

Appendix A.1. Functions used in **`arruda_wypiwyg.jl`**

`arrboy`$(G, N_{ch}, ILF, \lambda_u, flagTest = 1)$
Arruda-Boyce model.
Given the material parameters and the Inverse Langevin function returns the Cauchy stress (σ_u) corresponding to given λ_u computed with the 8-chain model
Input: $\quad \lambda_u :: Array\{Float64, 1\}$: Test stretches. $\qquad\qquad ILF :: Function$: Inverse Langevin function $\qquad\qquad \lambda_u :: Array\{Float64, 1\}$: stretches   Optional: $flagTest :: Int64$: Flag specifying uniaxial $(= 1)$, biaxial $(= 2)$ or pure shear $(= 3)$ test   Output: $\quad \sigma_u :: Array\{Float64, 1\}$: Cauchy stress for λ_u computed with the 8-chain model

`ffromModel`$(\lambda_u, \sigma P_u, flagTest, flagStress = 1)$
This function interpolates the points $\left\{ \widehat{\lambda}_{ci}, \widehat{f}_{ci} \right\}$, which have been previously computed from $\left\{ \widehat{\lambda}_{ui}, \widehat{\sigma P}_{ui} \right\}$ using the function `ffromtests_points`
Input: $\quad G, N_{ch} :: Float64$: Material parameters. $\qquad\qquad \sigma P_u :: Array\{Float64, 1\}$: Cauchy or Nominal stress corresponding to λ_u. $\qquad\qquad flagTest :: Int64$: Flag which specifies uniaxial $(= 1)$, biaxial $(= 2)$ or pure shear $(= 3)$ test   Optional: $flagStress :: Int64$: Specifies whether the stress introduced is Cauchy (1) or nominal (2) Output: $\quad f :: Function$: Cubic spline function $f(\lambda_{ch})$ from $\left(\widehat{\lambda}_{ui}, \widehat{\sigma P}_{ui} \right)$ for test indicated by $flagTest$

ffromtests_points($\lambda_u, \sigma P_u, flagTest, flagStress = 1$)
Computes the points $\left\{ \widehat{\lambda}_{ci}, \widehat{f}_{ci} \right\}$ from $\left\{ \widehat{\lambda}_{ui}, \widehat{\sigma P}_{ui} \right\}$ for a specified test.

Input:	$\lambda_u :: Array\{Float64, 1\}$: Test stretches
	$\sigma P_u :: Array\{Float64, 1\}$: Cauchy or nominal stress corresponding to λ_u
	$flagTest :: Int64$: Flag specifying uniaxial ($= 1$), biaxial ($= 2$) or pure shear ($= 3$) test
Optional:	$flagStress :: Int64$: Specifies whether the stress introduced is Cauchy (1) or nominal (2)
Output:	$\widehat{\lambda}_{ci} :: Array\{Float64, 1\}$: Points of λ_{ch} corresponding to $\widehat{\lambda}_{ui}$ (test stretches)
	$\widehat{f}ci :: Array\{Float64, 1\}$: Values of $f(\lambda_{ch})$ at $\widehat{\lambda}_{ci}$ from $\widehat{\lambda}_{ui}$, and $\widehat{\sigma P}_{ui}$ (test points)

csplinef($x, y, EndC1 = 2, EC1 = 0, EndC2 = 2, EC2 = 0$)
Returns a cubic spline which interpolates the points x and y for given boundary conditions

Input:	$x :: Array\{Float64, 1\}$: Abcisae vector, increasing
	$y :: Array\{Float64, 1\}$: Ordinates corresponding to x.
Optional:	$EndC1 :: Int64$: Initial boundary condition is first ($= 1$) or second ($= 2, def$) derivative
	$EndC2 :: Int64$: Final boundary condition is first ($= 1$) or second ($= 2, def$) derivative
	$EC1 :: Float64$: Value of prescribed bound. conf. at the beginning (0 by default).
	$EC2 :: Float64$: Value of prescribed bound. conf. at the end (0 by default).
Output:	$y_{cs} :: Function$: Local cubic spline
	(its input has to be a Float64. If vector evaluation is required, broadcasting can be used)

sigma_wypiwyg($\lambda_u, f_{ch}, flagTest = 1$)
Returns the Cauchy stress corresponding to λ_u for the $flagTest$ specified.

Input:	$\lambda_u :: Array\{Float64, 1\}$: Stretches at which the Cauchy stress is to be determined
	$\sigma P_u :: Array\{Float64, 1\}$: Cauchy or nominal stress corresponding to λ_u
Optional:	$flagTest :: Int64$: Flag which specifies uniaxial ($= 1$), biaxial ($= 2$) or pure shear ($= 3$) test.
Output:	$\sigma_w :: Array\{Float64, 1\}$: Cauchy stress computed using $f(\lambda_{ch})$

Appendix A.2. Functions used in **arruda_wypiwyg_treloar.jl**

readCurve($file$)
Returns two vectors x and y containing the first and the second column contained in file $file$

Input:	$file :: String$: A String with the name of the data file
	The data file has two columns: (1) stretch data and (2) stress data
Output:	$x :: Array\{Float64, 1\}$: Data from first column of $file$ (stretches)
	$y :: Array\{Float64, 1\}$: Data from second column of $file$ (stress)

`ffromtests`$(\lambda_u, \sigma P_u, \lambda_{ublock}, flagTest, flagStress = 1)$
Returns the function $f(\lambda_{ch})$ using the function `rational_joint`
The function $f(\lambda_{ch})$ is a composition of a B-spline and a rational function.
Bspline part: Computed with the function `bsplinefdf` from the points $\left\{\widehat{\lambda}_{ci}, \widehat{f}_{ci}\right\}$,
which have been previously obtained from $\left\{\widehat{\lambda}_{ui}, \widehat{\sigma P}_{ui}\right\}$ using the function `ffromtests_points`.
Rational part: Rational function with C^1continuity with the B-spline at last exp. point $\left\{\widehat{\lambda}_{cend}, \widehat{f}_{cend}\right\}$.
The rational function has its assymptote at λ_{lock}

Input:	$\lambda_u :: Array\{Float64, 1\}$: Test stretches
	$\sigma P_u :: Array\{Float64, 1\}$: Cauchy or nominal stress corresponding to λ_u
	$flagTest :: Int64$: Flag specifying uniaxial $(= 1)$, biaxial $(= 2)$ or pure shear $(= 3)$ test
Optional:	$flagStress :: Int64$: Specifies whether the stress introduced is Cauchy (1) or nominal (2)
Output:	$f :: Function$: function $f(\lambda_{ch})$ computed from $\left\{\widehat{\lambda}_{ui}, \widehat{\sigma P}_{ui}\right\}$

`ffromtests`$(\lambda_u, \sigma P_u, \lambda_{ublock}, flagTest, flagStress = 1)$
Computes the points $\{\widehat{\lambda}_{ci}, \widehat{f}_{ci}\}$ from $\{\widehat{\lambda}_{ui}, \widehat{\sigma P}_{ui}\}$ for a specified test

Input:	$\lambda_u :: Array\{Float64, 1\}$: Test stretches.
	$\sigma P_u :: Array\{Float64, 1\}$: Cauchy or nominal stress corresponding to λ_u
	$flagTest :: Int64$: Flag specifying uniaxial $(= 1)$, biaxial $(= 2)$ or pure shear $(= 3)$ test
Optional:	$flagStress :: Int64$: Specifies whether the stress introduced is Cauchy (1) or nominal (2)
Output:	$\widehat{\lambda}_{ci} :: Array\{Float64, 1\}$: Points of λ_{ch} corresponding to each of the $\widehat{\lambda}_{ui}$ (test stretches).
	$\widehat{f}ci :: Array\{Float64, 1\}$: Evaluation of $f(\lambda_{ch})$ at $\widehat{\lambda}_{ci}$

`rational_joint`$(x, y, x_l, x_{li}, cond1 = 3, cond2 = 1)$
Returns a piecewise function formed of a B-spline and a rational function.
Bspline part: Computed with the function `bsplinefdf` from the points $(\widehat{x}_i, \widehat{y}_i)$.
It uses the conditions $cond1$ and $cond2$ and a number of vertices specified by the user
Rational part: with C^1continuity with B-spline at $\{\widehat{x}_l, \widehat{y}_l\}$ and assymptote at x_{li}.

Input:	$x :: Array\{Float64, 1\}$: Abcisae vector, increasing
	$y :: Array\{Float64, 1\}$: Ordinates corresponding to x.
	$xl :: Float64$: Connecting location between B-spline and rational function
	$xli :: Float64$: Location of the asymptote
Optional:	$cond1 :: Int64$: Flag used to call `bsplinefdf` (value 3 by default)
	$cond2 :: Int64$: Flag used to call `bsplinefdf` (value 1 by default)
Output:	$rational\_joint :: Function$: Piecewise function

bsplinefdf$(x, y, cond1 = 1, cond2 = 1, nvertices = 11)$
Returns B-spline and its derivative computed from $\{x, y\}$ points with smoothing conditions

Input:	$x :: Array\{Float64, 1\}$: Abcisae vector, increasing
	$y :: Array\{Float64, 1\}$: Ordinates corresponding to x.
	$xl :: Float64$: Connecting location between B-spline and rational function
	$xli :: Float64$: Location of the asymptote
Optional:	$cond1 :: Int64$:Flag used to determine the point weights matrix $\boldsymbol{W}$
	$cond1 = 1$ (Default). Penalizes all the vertices with a value
	and increases penalization at the beginning and at the end.
	$cond1 = 2$. No penalization
	$cond1 = 3$ (Default). Same as $cond1 = 1$ but also penalizes
	more those vertices in which 1st derivative is negative
	$cond2 :: Int64$: Flag used to determine the penalization weights matrix $\boldsymbol{\Omega}$
	$cond2 = 1$. Increased penalization only at the end
	$cond2 = 2$. Increased penalization at the beginning and at the end
	$cond2 = 3$. Increased penalization only at the beginning
	$cond2 = 4$. Uniform penalization
	$nvertices = 11$: Number of vertices of the control polygon
Output:	$f_{bs} :: Function$: B-spline function
	$df_{bs} :: Function$: B-spline derivative function (for constitutive tangents)